# Model predictive control for multimode power-split hybrid electric vehicles: Parametric internal model with integrated mode switch and variable meshing losses

Mechanism and Machine Theory 192 (2024) 105543

Contents lists available at ScienceDirect

Mechanism and Machine Theory

journal homepage: www.elsevier.com/locate/mechmt

Research paper

# Model predictive control for multimode power-split hybrid electric vehicles: Parametric internal model with integrated mode switch and variable meshing losses

Antonella Castellano [a], Pietro Stano [b], Umberto Montanaro [b], Marco Cammalleri [a,*], Aldo Sorniotti [c]

[a] Department of Engineering, University of Palermo, Italy
[b] Centre for Automotive Engineering, University of Surrey, Guildford, UK
[c] Department of Mechanical and Aerospace Engineering, Politecnico di Torino, Italy

ARTICLE INFO

*Keywords:*
Power-split hybrid electric vehicle
Energy management strategy
Model predictive control
Multimode transmission
Planetary gear
Meshing loss

ABSTRACT

Model predictive control (MPC) is one of the most promising energy management strategies for hybrid electric vehicles. However, owing to constructive complexity, the multimode power-split powertrain requires dedicated mathematical tools to model the mode switch and transmission power losses within the internal model of the controller. Thus, the transmission losses are usually neglected and the mode switch is optimised through offline simulations. This paper proposes an MPC internal model relying on a parametric approach available in the literature, which provides a unique formulation for modelling any power-split transmission and assesses the transmission meshing losses. The objectives, which cover a gap in the literature, are: 1) to integrate the discrete problem of the mode switch in a continuous formulation of the internal model; 2) to compare MPC internal models with different complexity, and evaluate how the consideration of meshing losses and efficiency of the electric machines affect the controller performance. The results on a case study vehicle, i.e., the Chevrolet Volt, suggest that a simplified internal model deteriorates the fuel consumption performance by less than 2 %, while the integrated mode switch is comparable to the offline strategy.

## 1. Introduction

Hybrid electric vehicles (HEVs) are increasingly standing out in the automotive market as an effective solution towards more sustainable mobility to face rising greenhouse gases and pollutant emissions [1]. Amongst the available hybrid technologies, the power-split powertrain is the most promising one [2,3]. The core of this architecture is the power-split continuously variable transmission (PS-CVT) that couples the internal combustion engine (ICE) and the final drive. A PS-CVT consists of a power-split unit (PSU), including one or more planetary gear trains (PGs) and, optionally, ordinary gear trains (OGs). Since the PSU has two kinematic degrees of freedom, the ICE speed is decoupled from the vehicle speed by deploying two electric motor-generators (MGs) in the electric unit as a continuously variable unit to continuously vary the transmission speed ratio. As a result, the engine can operate at its best efficiency

* Corresponding author.
*E-mail address:* marco.cammalleri@unipa.it (M. Cammalleri).

https://doi.org/10.1016/j.mechmachtheory.2023.105543
Received 29 September 2023; Received in revised form 17 November 2023; Accepted 17 November 2023
Available online 24 November 2023

**Nomenclature**

*Acronyms*

| | |
|---|---|
| CS | compound-split mode |
| EMS | energy management strategy |
| FR | fixed-ratio mode (parallel mode) |
| HEV | hybrid electric vehicle |
| ICE | internal combustion engine |
| IM | internal model |
| IS | input-split mode |
| MG | motor-generator |
| MPC | model predictive control |
| OG | ordinary gear train |
| OOL | engine optimal operating line |
| PG | planetary gear train |
| PS-CVT | power-split continuously variable transmission |
| PSU | power-split unit |
| SOC | state of charge |

*Subscripts*

| | |
|---|---|
| *C, R, S* | carrier, ring gear and sun gear |
| *in, out, i, o* | external ports of the PSU |

*Symbols*

| | |
|---|---|
| $k_j$ | gear ratio of the OG on the generic shaft *j* |
| $P_j$ | power flowing through the generic shaft *j* |
| $p_{LOSS}$ | meshing power losses as a fraction of the input power |
| $T_{ICE}, T_{MGA}, T_{MGB}$ | actuators torque |
| $T_j$ | torque applied to the generic shaft *j* |
| $\Theta$ | torque applied to the shaft *out* as a fraction of the input torque (overall torque ratio) |
| $\tau$ | overall speed ratio |
| $\tau_j$ | speed ratio of the generic shaft *j* |
| $\tau_{\#j}$ | overall speed ratio for which the shaft *j* is stationary (nodal ratio) |
| $\tau_{j\#k}$ | speed ratio of the shaft *j* when the shaft *k* is stationary (corresponding speed ratio) |
| $\Psi$ | Willis' ratio of a PG |
| $\omega_j$ | rotational speed of the generic shaft *j* |
| $\dot{\omega}_j$ | angular acceleration of the generic shaft *j* |

condition, as in series hybrid configurations. Moreover, the engine power can be transferred to the electric unit for battery recharging but also to the final drive for traction, as in parallel hybrid set-ups.

Besides the simplest power-split layout implemented with a single PG, a system of brakes and clutches can be included in a PSU with two or more PGs to realise multimode PS-CVTs [4–6]. Appropriate switching the state of each brake and clutch can prevent the rotation of some of the PSU shafts or change the connection between them. Thus, multiple power-split layouts are available to be selected according to the current driving condition, to keep the ICE close to its most efficient operation by complying with the speed and torque constraints of the electric machines. Therefore, multimode operations enhance high-efficiency performance in several scenarios without oversizing the electric unit. The counterpart of this flexibility is the higher constructive complexity [7], which requires dedicated mathematical tools to model the multimode PS-CVTs during the design and analysis stages. Moreover, the mode shift complicates the energy management strategy (EMS) and powertrain control system.

Implementing an effective EMS is vital to achieve the full benefits of HEVs. An actual reduction in fuel consumption and emissions can be obtained only if the demanded power is instantaneously split between the engine and the battery so as to keep the ICE operating as efficiently as possible, minimise the powertrain power losses, and maintain the battery state of charge (SOC) around a desired value. For this purpose, several EMSs for HEVs have been developed [8–10]. They are commonly divided into rule-based and optimisation-based EMSs. The former determine the control actions by relying on a set of rules derived from heuristics or from the prior knowledge of the optimal solution obtained by optimisation-based algorithms. Consequently, rule-based EMSs are suitable for real-time implementation but often lead to a suboptimal solution. On the other hand, optimisation-based EMSs consist of establishing and solving a constrained optimisation problem based on the minimisation of a cost function. Some optimisation-based EMSs, such as dynamic programming, Pontryagin's minimum principle, simulated annealing, genetic algorithm, and game theory, are able to find a global optimum, but can be implemented only offline because of the high computational time and the need for prior knowledge of the driving cycle. On the contrary, other optimisation-based EMSs, such as the equivalent consumption minimisation strategy, model

predictive control (MPC), and reinforcement learning, are based on algorithms that can solve an instantaneous optimisation problem, potentially in real-time. Nonetheless, they result in a local optimum and require a simplified vehicle model that balances accuracy and computational effort.

Amongst the EMSs outlined above, we focus this research on MPC because of its capability to deal with complex multivariable constrained problems on the basis of the prediction of the system future state in a receding horizon framework [11–13]. Although the quality of the optimisation outcome is strongly dependant on the quality of the prediction and information on the road/traffic conditions ahead, MPC does not require knowing the full driving cycle in advance, as in global optimisation-based EMSs. Instead, such information on the route can be instantaneously acquired by the vehicle sensors, global positioning systems, and intelligent transportation systems. As a result, the implementation of predictive controllers for automotive applications, benefitting from different typologies of preview information, is a clear trend in recent research, not only for EMS development [14–17]. In this regard, a case study on a power-split HEV presented in [18], proved that a 4 % gain in fuel saving can be obtained if MPC is adopted in place of the EMS developed by the vehicle manufacturer. Nonetheless, also the accuracy of the vehicle model on which the optimisation algorithm is based may affect the controller performance in terms of both fuel saving and computational time. Thus, the internal model implemented within the control strategy should be complex enough to guarantee optimal powertrain operation in real time, while also involving a low running time.

The latest contributions available in the literature on MPC strategies applied to power-split HEVs mainly focus on more reliable predictions of future driving conditions [19–31] and more efficient optimisation algorithms [27,28,31–39]. Some of these contributions deal with multimode PS-CVTs [23–25,27,30,31,34–36], but only Oncken et al. [30] and Wang et al. [36] address in detail the mode shift strategy. The major challenge of a multimode PS-CVT is that, besides the continuous optimisation to allocate power amongst the thermal and electric units, additional discrete optimisation is required for mode selection. To overcome this issue, a two-level real-time-capable controller consisting of a discrete mode path planning and a continuous MPC is proposed in [30]. The solution presented in [36] is the only one that integrates the mode shift strategy into the MPC framework through a novel receding horizon algorithm combining MPC with dynamic programming. Its real-time implementation has not been tested. In the other cases, the mode shift strategy has relied on precalculated mode shift maps, often obtained through offline optimisation, which provide the optimal operating mode on the basis of the current driving conditions, e.g., the actual vehicle speed and driver demanded torque. Then, the optimal mode is provided as an external input to the MPC EMS, which involves as many internal models as the number of available modes.

Moreover, the analysis of the literature reveals that, while considering the conversion power losses in the ICE, MGs, and the battery within the MPC internal model is well-established, the increased complexity of PS-CVTs hinders an adequate consideration of the transmission power losses. This is due to the intrinsic difficulty in evaluating PG power losses, which has been the subject of extensive studies, resulting in three main approaches: experimental investigation [40,41], elastohydrodynamic lubrication formulation of the contacting surfaces [42], and models using a constant or empirically estimated friction coefficient [43–48]. Due to the simplified formulation, the last approach is the most suitable for implementation within an MPC internal model. Only the power losses due to sliding friction in meshing pairs are often considered, as they are the most significant ones [40,41]. Nonetheless, even under this simplifying assumption, including an accurate assessment of the PSU meshing power losses in a MPC internal model is still challenging because it often involves case-specific formulations necessary to consider the actual power flow into each PG branch. As a result, the vast majority of the published research works neglect any power losses in the PGs of the PSU, while there are some attempts [22,28,38] to consider a global efficiency of the PSU. Still, they fail to consider the possibility of power flow reversal during regenerative braking or when an MG switches from motoring to generating operations and vice versa. To the authors' knowledge, the analysis of how the inclusion of the PSU power losses in the internal model can affect the MPC performance is not available in the literature.

As a result, two main gaps have emerged from the literature analysis on MPC for the EMS of power-split hybrid electric vehicles:

(1) the lack of integration of the discrete mode shift strategy within the MPC framework using a continuous formulation, which is essential to find the optimal profile of all the control inputs over the prediction horizon, including the mode selection, through a single optimal control problem;
(2) the lack of a comparative analysis of MPC internal models with different levels of complexity to assess how the accuracy of the internal model affects the controller performance.

To cover these identified gaps, this work proposes a novel MPC internal model for multimode PS-CVTs including a unique continuous formulation to integrate the mode switch control within the MPC framework. To this purpose, a unified parametric model for PS-CVTs already available in the literature [48–50] is rearranged to be used in the MPC problem. It relies on a universal formulation ruled by some functional parameters that can be univocally derived from any constructive layout [50]. Thus, changing the constructive layout, e.g., after a mode shift in a multimode PS-CVT, does not result in different equations, as it is for the other PS-CVT models available in the literature, but only in different functional parameters. Therefore, it is possible to model several modes within the same controller by introducing switch functions to consider the functional parameters variation. As a result, any preliminary offline optimisation is unnecessary for the mode shift strategy, which, instead, can be embedded within the receding horizon framework. Moreover, the same parametric model includes a fast approximated procedure to calculate the meshing losses in the PSU [48,51] as a function of the PSU operating point, without requiring any case-specific formulation depending on the power flows direction. Thus, such a model is suitable for MPC implementation. For the first time in the field of MPC-based EMS for power-split HEVs, the influence of variable PSU power losses is assessed by comparing internal models with different levels of complexity. The influence of actuators inertial load and MGs efficiency is also considered. The results of this comparison are useful to assess how neglecting some of these factors may affect the effectiveness of the EMS considered in the powertrain design phase, when some parameters are to be defined yet.

The remainder is organised as follows. Section 2 describes the universal formulation underpinning the parametric internal model, with some hints of its potential use in the design stage; Section 3 provides an example of application to the Voltec II, i.e., the multimode PS-CVT deployed on the second generation Chevrolet Volt, used as a case study; Section 4 describes the preliminary analysis that led to the definition of the internal models selected for the comparison; Section 5 defines the MPC problem formulation and presents a benchmarking control strategy; the results of the comparison of the MPCs embedding the different internal models and the benchmarking controller are presented and discussed in Section 6, while Section 7 concludes the paper.

## 2. Universal parametric model for PS-CVTs

The speed, torque, and power ratios between any two PSU shafts depend on how the PGs branches are connected, as well as on the PGs constructive ratio. Moreover, any OGs and the connections between the PSU internal shafts with the actuators and the wheels must also be considered to model the whole power-split driveline. The speed of PG branches is ruled by the Willis equation, while the torque ratios are assessed by the free body diagram of the ring gear, sun gear, carrier, and planet gears in most of PS-CVTs models available in the literature. Nonetheless, modelling any power-split powertrain with this approach requires equations suitable only to the analysed PS-CVT; whenever the PSU constructive arrangement changes, even just in terms of the connections between shafts, a different set of equations must be considered.

To outgrow the need for a case-specific formulation for PS-CVTs, a universal parametric model was proposed in [48–50]. Any PSU is modelled as a four-port device that some functional parameters can comprehensively characterise by ruling a set of universal equations for speed, torque and power ratios. The PSU external ports are connected to the ICE, the wheels, and the two electric MGs. They are indicated as port *in*, *out*, *i*, and *o*, respectively (Fig. 1).

The basic functional parameters underpinning the model are the nodal ratios and the corresponding speed ratios. The former are defined as the overall speed ratio $\tau = \omega_{out}/\omega_{in}$ achieved when the generic shaft $k$ in the PSU is stationary:

$$\tau_{\#k} = \left.\frac{\omega_{out}}{\omega_{in}}\right|_{\omega_k=0} \tag{1}$$

The latter are defined as any other speed ratio $\tau_j = \omega_j/\omega_{in}$ with $j \neq out$ achieved when the generic shaft $k$ is stationary:

$$\tau_{j\#k} = \left.\frac{\omega_j}{\omega_{in}}\right|_{\omega_k=0} \tag{2}$$

Being speed ratios, these functional parameters are related to the Willis ratio of the PGs and the gear ratio of the OGs in the PSU. They are also affected by the state of any clutch included in a multimode PS-CVT arrangement. Nonetheless, an automated matrix approach was proposed in [50] to identify the functional parameters from the constructive layout of any PSU, the number of PGs and modes notwithstanding. The strength of this parametric approach is the capability of modelling any PS-CVT relying on the same set of equations ruled by the functional parameters. The numerical values of the latter are the only difference amongst different PSUs, or between two modes of the same PSU. Moreover, the nodal ratios $\tau_{\#i}$ and $\tau_{\#o}$, also called mechanical points, and the corresponding speed ratios $\tau_{o\#i}$ and $\tau_{i\#o}$ referred to the shafts connected to the electric unit are sufficient to address the kinematics and kinetostatics of the four PSU external shafts.

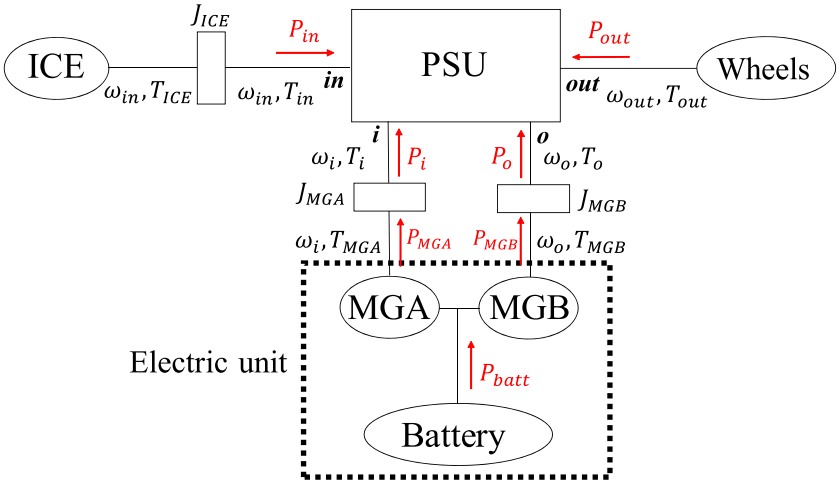


**Fig. 1.** Universal schematisation for power-split powertrain. Red arrows show the direction of positive power flows.

### 2.1. Kinematics, torques, and power flows of the power-split hybrid electric powertrain

The mathematical treatment proposed in [48,50] was presented in a dimensionless form since the speed, torque, and power of the ports *out*, *i*, and *o* were expressed as a fraction of speed, torque, and power of the shaft *in*, owing to the two degrees of freedom of the PSU. Therefore, in this paper, the previous mathematical formulation is rearranged to obtain a dimensional model that outputs the operating point of each MG as a function of the vehicle speed, the driver's demand, and ICE operations resulting from the EMS, in order to assess fuel consumption and battery SOC. Any component in the PSU is considered as a rigid body and the inertia of shafts and gears is neglected.

The speed of the electric MGs is:

$$\begin{aligned}\omega_i &= \frac{\tau_{i\#o}}{\tau_{\#o}-\tau_{\#i}}(\omega_{out}-\tau_{\#i}\omega_{in})\\ \omega_o &= \frac{\tau_{o\#i}}{\tau_{\#i}-\tau_{\#o}}(\omega_{out}-\tau_{\#o}\omega_{in})\end{aligned} \tag{3}$$

$\omega_{out}$ is directly proportional to the vehicle speed. Equivalently, accelerations are ruled by the same relations:

$$\dot{\omega_i} = \frac{\tau_{i\#o}}{\tau_{\#o}-\tau_{\#i}}(\dot{\omega_{out}}-\tau_{\#i}\dot{\omega_{in}})\dot{\omega_o} = \frac{\tau_{o\#i}}{\tau_{\#i}-\tau_{\#o}}(\dot{\omega_{out}}-\tau_{\#o}\dot{\omega_{in}}) \tag{4}$$

The mechanical power on the shafts *i* and *o* can be assessed by adding to the power transmitted in ideal conditions a contribution to consider the friction power losses in the PSU meshing gears:

$$\begin{aligned}P_i &= P_{i,id}+\Delta P_{i,LOSS}\\ P_o &= P_{o,id}+\Delta P_{o,LOSS}\end{aligned} \tag{5}$$

where $P_{i,id}$ and $P_{o,id}$ are the ideal power flows, ruled only by the mechanical points:

$$\begin{aligned}P_{i,id} &= \frac{1}{\tau_{\#i}-\tau_{\#o}}(\omega_{out}-\tau_{\#i}\omega_{in})(\tau_{\#o}T_{out}-T_{in})\\ P_{o,id} &= \frac{1}{\tau_{\#o}-\tau_{\#i}}(\omega_{out}-\tau_{\#o}\omega_{in})(\tau_{\#i}T_{out}-T_{in})\end{aligned} \tag{6}$$

The contribution due to the meshing losses is:

$$\begin{aligned}\Delta P_{i,LOSS} &= -\frac{\omega_i T_{in}}{\tau_{i\#o}}\left[p_{LOSS}+\frac{\partial p_{LOSS}}{\partial\tau}(\tau_{\#o}-\tau)\right]\\ \Delta P_{o,LOSS} &= -\frac{\omega_o T_{in}}{\tau_{o\#i}}\left[p_{LOSS}+\frac{\partial p_{LOSS}}{\partial\tau}(\tau_{\#i}-\tau)\right]\end{aligned} \tag{7}$$

where $p_{LOSS}$ is the power loss as a fraction of the input power. $p_{LOSS}$ can be evaluated by the approximated method introduced in [48] and further described in Section 3.13.1. If the PSU losses are neglected, $\Delta P_{i,LOSS} = \Delta P_{o,LOSS} = 0$. In Eqs. (5), (7), $T_{in}$ is the torque on the PSU input shaft, while $T_{out}$ is the torque on the PSU output shaft, depending on the demanded torque, $T_{dem}$, consisting of the aerodynamic, rolling, grade and inertial resistances as follows:

$$T_{dem} = -\left(\frac{1}{2}c_d A_f \rho_a V_{veh}^2 + f_r mg\cos\gamma + mg\sin\gamma + \delta m a_{veh}\right)R_w \tag{8}$$

where $c_d$ is the drag coefficient, $A_f$ is the vehicle frontal area, $\rho_a$ is the air density, $V_{veh}$ is the vehicle speed, $f_r$ is the rolling friction coefficient, $m$ is the vehicle mass, $g$ is the gravitational acceleration, $\gamma$ is the road gradient, $\delta$ is the coefficient that accounts for the wheels moment of inertia, $a_{veh}$ is the vehicle acceleration, and $R_w$ is the wheel rolling radius. For the power sign convention indicated in Fig. 1, whereby the power is positive if entering the PSU, $T_{out}$ is negative during vehicle traction and positive during braking. To consider the operation of the friction brakes to avoid MGs saturation during regenerative braking, $T_{out}$ is considered as:

$$T_{out} = T_{dem} - T_{brake} \tag{9}$$

where $T_{brake} > 0$ is the friction brake torque.

The torque on the shafts *i* and *o* of the PSU can be assessed by dividing Eqs. (5) by Eqs. (3), while the mechanical torque at the actuators level is affected by their moments of inertia, $J_{ICE}$, $J_{MGA}$, and $J_{MGO}$:

$$T_{ICE} = T_{in} + J_{ICE}\dot{\omega_{in}} T_{MGA} = T_i + J_{MGA}\dot{\omega_i} T_{MGB} = T_o + J_{MGB}\dot{\omega_o} \tag{10}$$

Once the ICE operating point is known, the fuel rate can be assessed from the ICE efficiency map, as follows:

$$\dot{m}_{fuel} = \frac{\omega_{in} T_{ICE}}{H_{LHV} \cdot \eta_{ICE}} \tag{11}$$

where $H_{LHV}$ is the fuel lower heating value and $\eta_{ICE}$ is the engine efficiency, which is a function of the ICE speed and torque.

The electric power of each MG depends on the mechanical power delivered or absorbed and on its efficiency $\eta_{MGA}$ or $\eta_{MGB}$:

$$\begin{aligned} P_{MGA,el} &= \omega_i T_{MGA} \eta_{MGA}^{-sign(\omega_i T_{MGA})} \\ P_{MGB,el} &= \omega_o T_{MGB} \eta_{MGB}^{-sign(\omega_o T_{MGB})} \end{aligned} \tag{12}$$

For an ideal battery, the net power flow is:

$$P_{batt,id} = P_{MGA,el} + P_{MGB,el} \tag{13}$$

A simplified battery model widely adopted in the relevant literature considers an equivalent circuit with a voltage source in series with a resistor. The battery efficiency $\eta_{batt}$ can be assessed as:

$$\eta_{batt} = \frac{V_{OC} + \sqrt{V_{OC}^2 - 4\left|P_{batt,id}\right| R_{batt}}}{2V_{OC}} \tag{14}$$

where $V_{OC}$ is the open-circuit voltage and $R_{batt}$ is the battery internal resistance. Then, the actual battery power is:

$$P_{batt} = P_{batt,id} \eta_{batt}^{-sign\left(P_{batt,id}\right)} \tag{15}$$

The battery current can be expressed as the ratio between the battery power and the output voltage determined by Kirchhoff's voltage law. Then, the rate of the battery state of charge is the opposite of the ratio between the battery current and the battery capacity $Q_{batt}$:

$$\dot{SOC} = -\frac{V_{OC} - \sqrt{V_{OC}^2 - 4P_{batt} R_{batt}}}{2R_{batt} Q_{batt}} \tag{16}$$

### 2.2. Hints for a hierarchical and modular design for PS-CVTs

The integration of the model described in Section 2.1 within the MPC framework paves the path for the selection of the optimal functional parameters in the design stage. Indeed, a comprehensive assessment of any PS-CVT behaviour is performed by requiring only the a priori knowledge of the functional parameters, which are univocally defined for an existing PSU. However, the same set of functional parameters can be achieved by several constructive arrangements. The equations reported in Section 2.1 are general and do not depend on the PSU constructive arrangement. Thus, for a given vehicle, it is possible to simulate the MPC-based EMS by assuming upstream different values for the functional parameters, achieving a swift evaluation of how different functional parameters affect fuel consumption over a simulation of a typical driving scenario. The strength of this approach is that the powertrain behaviour is comprehensively evaluated even though the PS-CVT has not been synthesised yet. Furthermore, the procedure applies also to multimode operations by modelling the functional parameters through continuous switch functions, as explained in Section 3.1.

A design procedure for PS-CVTs based on the parametric model was introduced in [49]. The aim was to provide a tool for a hierarchical and modular design, in contrast to the mere explorative approach usually adopted in the literature. The proposed approach prioritises selecting the mechanical points to minimise the size of the electric unit, which is usually the most expensive equipment. This is possible because the only mechanical points are sufficient to fully define the power flows of the electric unit (see Eqs. (6)). Hence, the MGs can be selected. The same mechanical points lead to the definition of a PSU design chart, by which the PG Willis ratio can be chosen to achieve the PG synchronism within the desired PSU working range. In this way, since the meshing losses in a PG are null at its synchronism, they are minimised within the whole working range. Lastly, selecting the corresponding speed ratios leads to the sizing of the OGs necessary to comply with the maximum speed and torque of the MGs.

Application examples were proposed in [49,52], but a rigorous procedure for selecting the optimal functional parameters for a given vehicle and ICE is still missing. Nonetheless, selecting the optimal functional parameters is out of the scope of this work. Instead, the model of this section is used as the internal model for the MPC formulation for the EMS problem of an existing multimode power-split powertrain.

## 3. Application on the multimode Voltec II

For any existing power-split HEV, the parametric model described in Section 2.1 can be used as the internal model for MPC formulation, after identifying the PSU functional parameters for each transmission mode through the procedure [50], assessing the power losses with the method [48], and including the ICE and MGs efficiency maps. The resulting constrained nonlinear optimisation problem must involve continuously differentiable constraints and objective functions if gradient-based optimisation methods are used

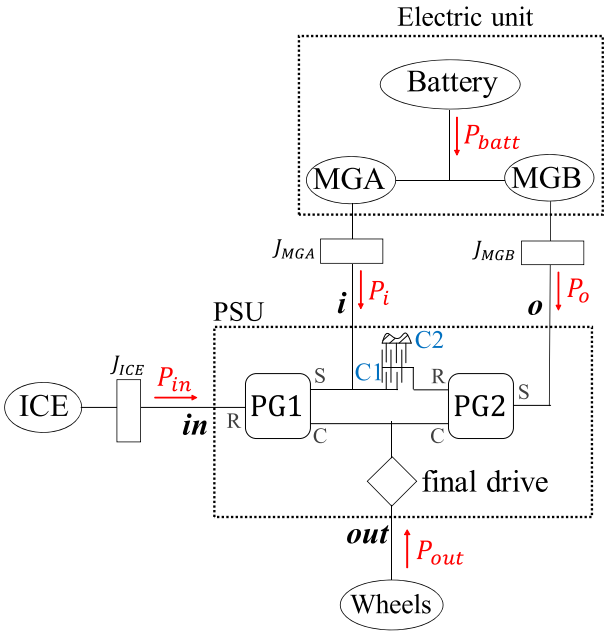


**Fig. 2.** Functional layout for Chevrolet Volt II power-split hybrid electric powertrain. R, S and C indicate PGs ring gear, sun gear, and carrier. C1 is a clutch, C2 is a brake.

**Table 1**
Chevrolet Volt II parameters derived from [53–55].

| Component | Symbol | Parameter | Value |
|---|---|---|---|
| Vehicle | $m_0$ | Unladen vehicle mass | 1607 kg |
| | $c_d$ | Drag coefficient | 0.28 |
| | $A_f$ | Frontal area | 2.20 $m^2$ |
| | $f_r$ | Rolling friction | 0.011 |
| | $\delta$ | Coefficient of wheels inertia | 1.04 |
| | $R_w$ | Wheel radius | 0.32 m |
| ICE | $P_{ICE}^{max}$ | Maximum power | 75 kW |
| | $T_{ICE}^{max}$ | Maximum torque | 140 Nm |
| | $\omega_{ICE}^{max}$ | Maximum speed | 6000 rpm |
| | $J_{ICE}$ | Moment of inertia | 0.04 $kgm^2$ |
| MGA / MGB | $P_{MGA}^{max}$ / $P_{MGB}^{max}$ | Peak power | 48 / 87 kW |
| | $T_{MGA}^{max}$ / $T_{MGB}^{max}$ | Peak torque | 118 / 280 Nm |
| | $\omega_{MGA}^{max}$ / $\omega_{MGB}^{max}$ | Peak speed | 10,000 / 10,000 rpm |
| | $J_{MGA}$ / $J_{MGB}$ | Moment of inertia | 0.03 $kgm^2$ / 0.05 $kgm^2$ |
| Battery | $Q_{batt}$ | Battery capacity | 52 Ah |
| | $V_{OC}$ | Open circuit voltage | 355 V |
| | $R_{batt}$ | Internal resistance | 0.1 Ω |
| | $P_{batt}^{max}$ | Maximum battery power | 120 kW |
| PSU | $\Psi_1$ | PG1 Willis ratio | − 0.535 |
| | $\Psi_2$ | PG2 Willis ratio | − 0.481 |
| | $k_{fd}$ | Final drive ratio [-] | 0.379 |

to search for the optimal solution. Thus, a continuous formulation is required to switch the functional parameters, the PSU meshing losses, and the actuators maps.

This section shows an example of application to the multimode PS-CVT Voltec II, deployed on the second generation of the Chevrolet Volt [53,54]. This is an extended-range hybrid electric vehicle equipped with a large battery pack to ensure a significant range in pure electric driving. However, when the battery SOC reaches the minimum value of 16 %, a power-split hybrid charge-sustaining mode is activated, and the variation of the battery SOC is maintained within ±1 %. Only the charge-sustaining operation is considered in this study. Fig. 2 shows the powertrain power-split layout, and Table 1 lists the main vehicle parameters derived from [53–55]. The Willis ratio is defined as the ratio of the ring gear speed and the sun gear speed when the carrier is stationary.

The power-split transmission system of the Chevrolet Volt includes two PGs and a final drive. The final drive consists of a third PG with stationary ring gear and a chain drive; thus, it can be modelled as a fixed-ratio OG. The ring gear of PG1 is connected to the ICE,

**Table 2**
Clutches operations for mode shifts. X indicates engaged clutches.

| Mode | C1 | C2 |
|---|---|---|
| Input-split (IS) | | X |
| Parallel fixed-ratio (FR) | X | X |
| Compound-split (CS) | X | |

**Table 3**
Functional parameters of Voltec II.

| Mode | $\tau_{\#i}$ | $\tau_{\#o}$ | $\tau_{o\#i}$ | $\tau_{i\#o}$ |
|---|---|---|---|---|
| Input-split | 0.247 | 0 | 2.00 | −1.87 |
| Compound-split | 0.247 | 0.510 | 2.00 | 2.00 |

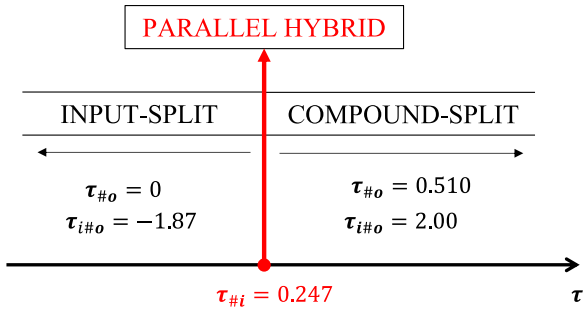


**Fig. 3.** Mode shift strategy in Voltec II based on the overall speed ratio $\tau$.

the sun gear to the electric machine MGA, and the carrier to the final drive, as the carrier of PG2. The sun gear of PG2 is connected to the electric machine MGB, while the ring gear can be connected to the PG1 sun gear and MGA by the clutch C1 or braked to the frame by the brake C2. Thus, the state of C1 and C2 determines which transmission mode is engaged, as indicated in Table 2. When only C2 is engaged, PG2 realises a fixed speed ratio between the final drive and MGB, while only PG1 has three branches with non-proportional speeds; therefore, the PSU operates in input-split mode. When only C1 is engaged, the MGA torque is allocated on both PGs and a compound-split mode is achieved. The functional parameters related to the two power-split modes have been identified in [56] and reported in Table 3.

Simultaneously engaging C1 and C2 results in a fixed-ratio parallel mode with the shaft $i$ stationary, whereby MGA is turned off and only MGB can operate for traction or regenerative braking. Moreover, the ICE speed $\omega_{in}^{FR}$ in parallel mode is proportional to the wheels speed by the inverse of the mechanical point $\tau_{\#i}$, which is the overall transmission ratio when the shaft $i$ is stationary by definition. Similarly, the corresponding speed ratio $\tau_{o\#i}$ univocally defines the speed $\omega_{o}^{FR}$ of the shaft $o$. Thus, the speed relations of Eqs. (3) valid for power-split operations can be replaced by the following ones in the parallel fixed-ratio mode:

$$\begin{aligned} \omega_{i}^{FR} &= 0 \\ \omega_{in}^{FR} &= \frac{\omega_{out}}{\tau_{\#i}} \\ \omega_{o}^{FR} &= \frac{\tau_{o\#i}}{\tau_{\#i}}\omega_{out} \end{aligned} \tag{17}$$

### 3.1. Switch functions for multimode operations

Although each power-split mode could be ideally selected for any overall transmission ratio $\tau$, multimode PS-CVTs are designed so as to drive in the input-split mode for lower ratios and in the compound-split mode for higher ratios. In this way, the power recirculation in the electric unit is limited and the compliance with the speed, torque, and power constraints of the electric MGs is ensured even if the electric unit is downsized [4,5]. Moreover, switching between modes is performed when the shafts involved in clutches operation have zero relative speed. In this way, the plates of clutches are prevented from slipping and a smooth synchronous mode shift is realised. In the case of Voltec II, the relative speed between the PG2 ring gear and MGA is zero at the mechanical point $\tau_{\#i}$, when MGA is stationary, similarly to the PG2 ring gear, which is either connected to MGA by C1 or braked to the frame by C2. Therefore, the mechanical point $\tau_{\#i}$ is not only the overall speed ratio at which parallel operation can be performed, but also the ratio at which mode

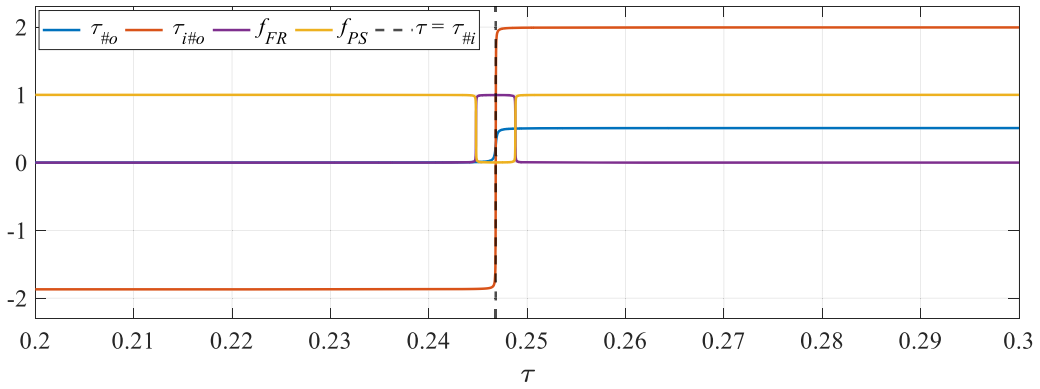


**Fig. 4.** Switch functions for the functional parameters and for power-split and parallel operation.

shift can occur, as shown in Fig. 3. Moreover, the functional parameters $\tau_{\#i}$ and $\tau_{o\#i}$ referred to the condition whereby the shaft $i$ is stationary are the same in both input-split and compound-split mode. On the contrary, the values of $\tau_{\#o}$ and $\tau_{i\#o}$ referred to the condition whereby the shaft $o$ is stationary are different (Table 3 and Fig. 3), since these speed ratios are affected by the state of the clutches on the shaft $i$ (see Fig. 2).

The described mode shift strategy can be embedded in the parametric model for the power-split operation of Section 2.1, by introducing continuous switch functions to model the switching functional parameters $\tau_{\#o}$ and $\tau_{i\#o}$. The continuous switch is obtained by the following functions of the overall speed ratio $\tau$:

$$\begin{aligned}\tau_{\#o} &= \frac{\tau_{\#o}^{CS}+\tau_{\#o}^{IS}}{2}+\frac{\tau_{\#o}^{CS}-\tau_{\#o}^{IS}}{\pi}atan(N_1(\tau-\tau_{\#i}))\\ \tau_{i\#o} &= \frac{\tau_{i\#o}^{CS}+\tau_{i\#o}^{IS}}{2}+\frac{\tau_{i\#o}^{CS}-\tau_{i\#o}^{IS}}{\pi}atan(N_2(\tau-\tau_{\#i}))\end{aligned} \tag{18}$$

where the apices *IS* and *CS* relate to the functional parameters of the input-split and compound-split mode, respectively. Moreover, to address also the fixed-ratio parallel mode within the same model, an additional set of switch functions is introduced:

$$\begin{aligned}f_{FR} &= \frac{1}{2}+\frac{2}{\pi^2}atan(N_3(-(\tau_{\#i}-\Delta)+\tau))\cdot atan(N_3((\tau_{\#i}+\Delta)-\tau))\\ f_{PS} &= \frac{1}{2}+\frac{2}{\pi^2}atan(N_3((\tau_{\#i}-\Delta)+\tau))\cdot atan(N_3((\tau_{\#i}+\Delta)-\tau))\end{aligned} \tag{19}$$

$f_{FR}$ and $f_{PS}$ are built so that the former is always zero except for a narrow neighbourhood of $\tau_{\#i}$ with a radius $\Delta$, when parallel mode occurs; conversely, the latter is zero in the neighbourhood of $\tau_{\#i}$ and 1 for any other $\tau$, where power-split operations are involved. The parameters $\Delta$, $N_1$, $N_2$, and $N_3$ must be selected to include $\tau_{\#o}$ and $\tau_{i\#o}$ switch within the range $\tau_{\#i}-\Delta \leq \tau \leq \tau_{\#i}+\Delta$ to avoid numerical errors in the solution of the MPC problem. Fig. 4 shows the trend of the switch functions of Eqs. (18) and (19).

The switch functions (19) replace the speed relations of Eq. (3) with the following ones:

$$\begin{aligned}\omega_i &= \omega_i^{FR}\cdot f_{FR}+\omega_i^{PS}\cdot f_{PS}\\ \omega_o &= \omega_o^{FR}\cdot f_{FR}+\omega_o^{PS}\cdot f_{PS}\end{aligned} \tag{20}$$

where $\omega_i^{PS}$ and $\omega_o^{PS}$ are those of Eq. (3). Similar relations rule the accelerations instead of Eq. (4).

### 3.2. Transmission meshing losses

The most common approaches for assessing meshing losses in PGs are based on the kinematic inversion to consider the efficiency of the corresponding ordinary gear train, achievable when the carrier is stationary. The ordinary efficiency can be easily evaluated as a function of gears parameters and friction conditions between teeth; then, it can be used to compute the meshing power losses in any other functioning state of the PG since the meshing losses depend only on the relative speed and transmitted torque. Nonetheless, case-specific formulations are necessary to correctly evaluate the global PG efficiency on the basis of the current power flows direction. The computational complexity in detecting the power flows and the subsequent losses is increased when a combination of multiple PGs and OGs is deployed, as in the PSU. Hence, including the PSU meshing losses in the MPC problem is far from trivial.

**Table 4**
PGs constructive parameters and loss factors for meshing losses assessment.

| PG | Willis ratio Ψ | Ordinary efficiency $\eta_0$ | Fixed-branch speed ratio $\psi$ | Loss factor $\eta$ |
|---|---|---|---|---|
| PG1 | $\psi_1 = -0.535$ | $\eta_{01} = 0.96$ | $\psi_1 = \Psi_1 = -0.535$ | $\eta_1 = \eta_{01} = 0.96$ |
| PG2 | $\psi_2 = -0.481$ | $\eta_{02} = 0.96$ | $\psi_2 = \frac{1}{1-\Psi_2} = 0.675$ | $\eta_2 = \frac{1-\Psi_2}{1-\Psi_2/\eta_{02}} = 0.987$ |

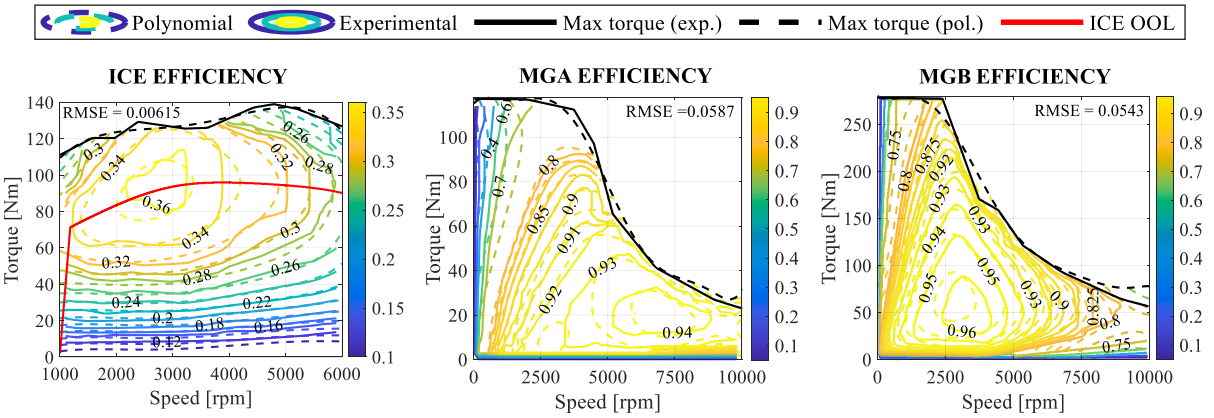


**Fig. 5.** Fitting results for actuators efficiency maps and maximum torques, with their respective root mean square error (RMSE).

Nonetheless, the need for a prior determination of the power flows was overcome in [48], which presented an approximated method with universal analytical relationships valid every time the ordinary efficiency is sufficiently high and the PG Willis ratio is lower than 0.5 or higher than 2. In other words, it can always be used, provided that the PG is well-designed. This method is based on the same parametric functional parameters outlined in Section 2 and led to Eq. (7) to evaluate the additional mechanical power that MGs should provide or absorb to compensate for the PSU meshing losses.

The PSU power losses of the Voltec II unit have already been assessed by the parametric approximated method in [48] as a fraction of the input power. To avoid repetition, the calculation procedure is omitted here. Nonetheless, the resulting equations in [48] need a mathematical rearrangement to obtain a continuous function of the overall speed ratio $\tau$ and overall speed ratio $\Theta = T_{out}/T_{in}$ to be included in Eq. (7) for MPC formulation. The following equation describes the Voltec II power losses normalised to the input power:

$$p_{LOSS} = (1-\eta_1)\left|1-\frac{\tau}{\tau_{\#i}(1-\psi_1)}\right| - \frac{1-\eta_2}{1-\psi_2}\left|\left(\Theta+\frac{1}{\tau_{\#i}}\right)\left[\frac{\tau_{\#o}}{\tau_{\#o}-\tau_{\#i}}(\tau-\tau_{\#i})-\psi_2\tau\right]\right| - (1-\eta_{fd})|\tau\Theta| \tag{21}$$

The first two terms are PG1 and PG2 meshing losses, dependant on their constructive arrangement, Willis ratio, and ordinary efficiency, according to Table 4. The third term is the loss in the fixed-ratio final drive, whose efficiency is $\eta_{fd} = 0.953$.

### 3.3. ICE and MGs efficiency maps

In contrast to the assessment procedure of the PSU meshing power losses, which is based on a physically consistent mathematical model that requires only the knowledge of the PSU constructive arrangement, the conversion power losses in the ICE and MGs are more often derived from experimental data. Thus, the efficiency of the actuators is available in the form of maps with scattered data that must be fitted to derive the continuous functions necessary for implementing gradient-based algorithms. Therefore, the ICE and MGs efficiency maps of the Chevrolet Volt available in [53,54] are approximated by fifth-order polynomial functions of their respective speed and torque:

$$\eta_k(\omega_k, T_k) = \sum_{m=0}^{5}\sum_{n=0}^{5-m} p_{mn}\omega_k^m T_k^n \tag{22}$$

where $k = ICE, MGA, MGB$. Moreover, a similar fitting is required for the maximum torque of the ICE and MGs, as a function of their respective speed, by using a single-variable n-th order polynomial:

$$T_k^{max}(\omega_k) = \sum_{m=1}^{n+1} p_m \omega_k^{n+1-m} \tag{23}$$

**Table 5**
Internal models for open-loop preliminary analysis.

| Internal Model | Inertial load | MGs efficiency | Meshing losses |
|---|---|---|---|
| OL_Baseline | Considered | Polynomial | Considered |
| OL_IdealMGE | Considered | $\eta_{MGA} = \eta_{MGB} = 1$ | Considered |
| OL_ConstantMGE | Considered | $\eta_{MGA} = 0.87;\ \eta_{MGB} = 0.9$ | Considered |
| OL_NoPSULosses | Considered | Polynomial | Neglected ($\Delta P_{i,LOSS} = \Delta P_{o,LOSS} = 0$) |
| OL_NoInertia | Neglected | Polynomial | Considered |

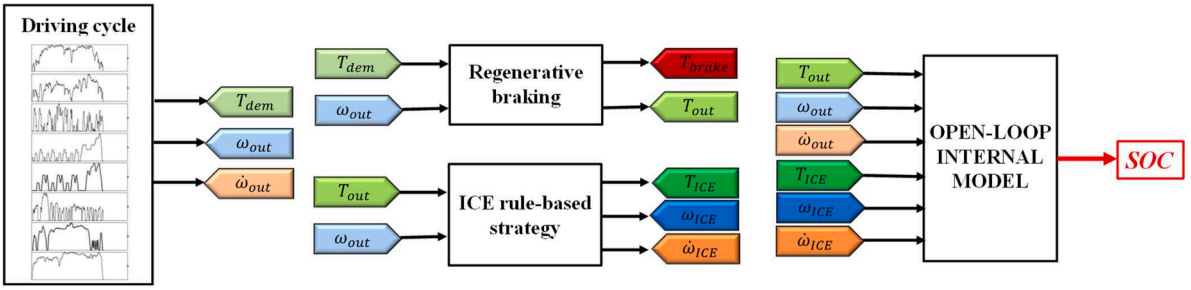


**Fig. 6.** Open-loop simulation framework for preliminary comparison.

**Table 6**
Characteristics of the simulated driving cycles.

| Driving cycle | Distance [m] | Duration [s] | Average speed [km/h] |
|---|---|---|---|
| Artemis Urban | 4874 | 993 | 17.7 |
| Artemis Road | 17,275 | 1082 | 57.5 |
| Artemis Motorway130 | 28,737 | 1068 | 96.9 |
| NEDC | 11,017 | 1180 | 33.6 |
| J10–15 | 4165 | 660 | 22.7 |
| UDDS | 11,997 | 1369 | 31.6 |
| HWFET | 16,503 | 765 | 77.7 |

A fourth-order polynomial was used for the ICE maximum torque, while a seventh-order polynomial was necessary for the MGA and MGB maximum torque. The fitting for the efficiency maps and maximum torque was performed by the MATLAB Curve Fitting toolbox. Fig. 5 shows the results of the interpolation.

## 4. Internal models definition by preliminary open-loop comparison

The accuracy and complexity of the vehicle internal model implemented within the MPC formulation might affect the EMS performance in terms of fuel saving and running time. Thus, a comparison of different internal models is proposed to assess the influence of the following factors:

1. PSU meshing losses;
2. MGs efficiency;
3. the inertial load of the actuators.

Although the PSU meshing losses are usually far lower than the power lost in the electro-mechanical conversion in the MGs and chemical-mechanical conversion in the ICE, they may become significant for considerable relative speed of PGs branches and high transmitted power. Moreover, their evaluation may help to select the optimal PSU constructive arrangement amongst those functionally equivalent in the design stage. Thus, evaluating their influence on the MPC performance may be interesting. Regarding the MGs efficiency, polynomial fitting is rather common in the literature. Nonetheless, it may be useful to assess the effects of a constant efficiency to be considered during the design stage, when the optimal functional parameters are not selected and the MGs are not sized yet. Lastly, the inertia of the actuators is nearly always neglected within the MPC formulation because its consideration would involve an additional state that complicates the problem and increases the computational effort.

To reduce the length of the simulation campaign, a preliminary analysis in an open-loop simulation framework is carried out to define the internal models worthy of investigation in the MPC framework. The internal models considered in the preliminary analysis are derived from the baseline model of Section 2.1, including the PSU meshing losses of Eq. (21), the polynomial form for MGs

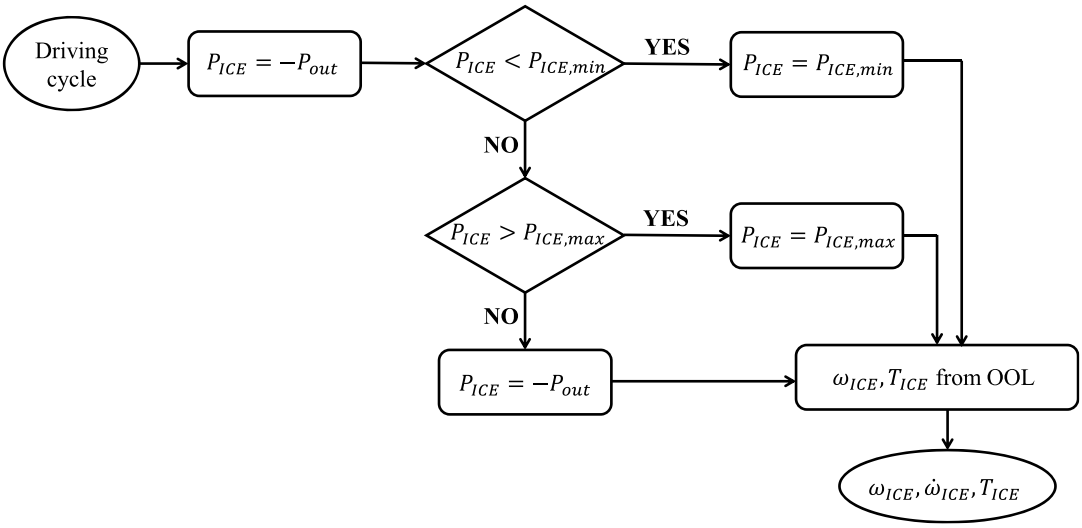


**Fig. 7.** Simplified rule-based strategy for ICE control in open-loop simulations.

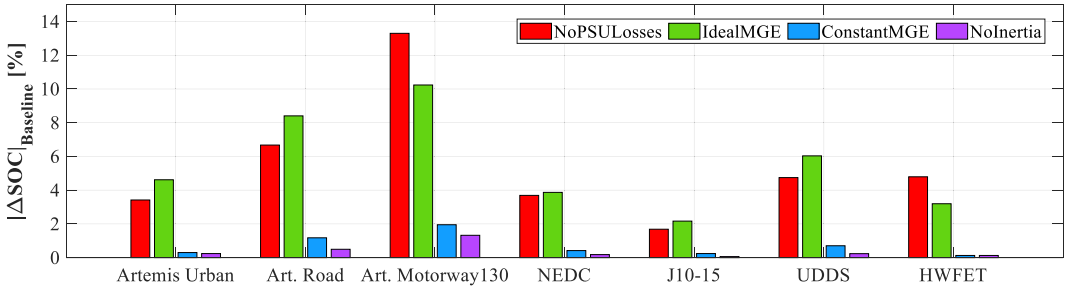


**Fig. 8.** SOC comparison resulting from the open-loop analysis in terms of variation from the Baseline SOC.

efficiency, and the inertial load of the actuators according to Eq. (10). Then, the complexity of the baseline model is reduced by modifying one of the three analysed factors at a time, see Table 5.

### 4.1. Open-loop simulation framework

A preliminary comparison of the five internal models listed in Table 5 is carried out by implementing the open-loop simulation framework shown in Fig. 6. The seven driving cycles listed in Table 6 are used to simulate typical conditions in terms of vehicle speed and acceleration, as well as the resulting demanded torque. A regenerative braking strategy is developed for the friction brakes, to prevent MGs saturation. During the deceleration phases, it assesses the resulting MGs torque values for the current demanded torque, considering the ICE idling operations. If the torque of one MG exceeds its maximum value for the current vehicle speed, this torque is saturated, and the resulting maximum torque $T_{out}$ recoverable on the *out* shaft is computed by inverting the torque equations that can be derived from the formulations in Section 2.1. Then, a simplified rule-based strategy is implemented to establish ICE operation. The core concept of the rule-based strategy, illustrated in Fig. 7, is to limit the battery involvement to simulate a realistic response of the Chevrolet Volt powertrain during the charge-sustaining operation. Thus, the ICE power is set equal to the output power during vehicle traction and the ICE operating points are kept as close as possible to the ICE optimal operating line (OOL) shown in Fig. 5. The acceleration of the engine is assessed by deriving the actual speed, which in a backward-facing model is the desired speed. If the demanded power overcomes the maximum ICE power, the ICE works at the maximum power, and the difference must be compensated by the battery; during regenerative braking, the ICE is kept idling and the recoverable mechanical energy is stored in the battery. The resulting ICE torque, speed, and acceleration are provided as input of each internal model defined by the equations of Sections 2 and 3 with the respective exceptions of Table 5. The internal model block simulates the PSU and electric unit operations and outputs the battery SOC, which is used as a benchmark index to compare the five internal models.

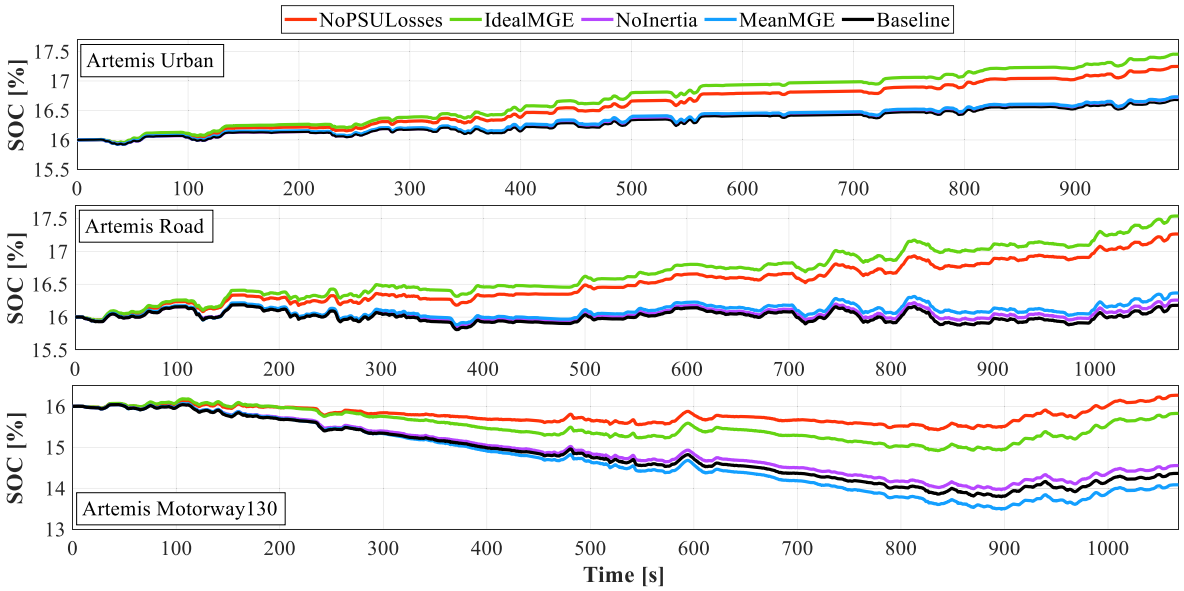


**Fig. 9.** SOC battery trend for Artemis driving cycles: open-loop comparison between the internal models of Table 5.

**Table 7**
Internal models to compare in the MPC framework.

| Internal Model | Inertial load | MGs efficiency | Meshing losses |
|---|---|---|---|
| MPC_IM1 | Neglected | $\eta_{MGA} = 0.87$ $\eta_{MGB} = 0.9$ | Neglected |
| MPC_IM2 | Neglected | Polynomial | Neglected |
| MPC_IM3 | Neglected | $\eta_{MGA} = 0.87$ $\eta_{MGB} = 0.9$ | Considered |
| MPC_IM4 | Neglected | Polynomial | Considered |

### 4.2. Results of the open-loop comparison and definition of MPC internal models

This preliminary comparison in open-loop aims to assess the impact of PSU power losses, MGs efficiency and actuators inertial load on the simulated powertrain response. Since the ICE operations derived from the rule-based strategy are the same for each internal model, only battery SOC is observed to quantify the deviation of each internal model from the baseline through the following percentage variation:

$$|\Delta SOC|_{Baseline,IM_j} = \frac{|SOC_{IM_j} - SOC_{Baseline}|}{SOC_{Baseline}} \cdot 100 \tag{24}$$

where $IM_j$ indicates the $j$th internal model. The comparison results are in Fig. 8, while Fig. 9 reports the trend of the battery SOC for each internal model in the Artemis driving cycles, by way of example.

The results of Figs. 8 and 9 suggest that the highest deviation from the baseline model is achieved when a unitary efficiency is assumed for the MGs efficiency. Moreover, neglecting PSU power losses implies a significant deviation as well, which is the largest in the high-speed driving cycles Artemis Motorway130 and HWFET. In both IdealMGE and NoPSULosses models, the final SOC is overestimated with respect to the baseline. On the contrary, omitting the actuators inertial load from the internal model does not result in significant SOC variation, especially in low-speed driving cycles. Similar considerations are valid for the internal model with a constant MGs efficiency in the place of polynomial maps.

Therefore, the results of this preliminary comparison suggest that it is worth investigating the impact of the PSU meshing losses in the MPC framework, while it is reasonable to neglect the actuators inertia to avoid computational complexity. Although the open-loop analysis reveals that a constant value could replace a polynomial model for the MGs efficiency, the influence of these two different approaches is deemed worthy of further analysis because, if the same trend is confirmed in the MPC framework, the traditional approach used in the literature based on the polynomial or experimental maps could be simplified into a constant efficiency, reducing the internal model complexity and thus the running time of the EMS solver. Given these considerations, the four internal models listed in Table 7 are considered in the MPC framework to assess the impact of PSU power losses and MGs efficiency.

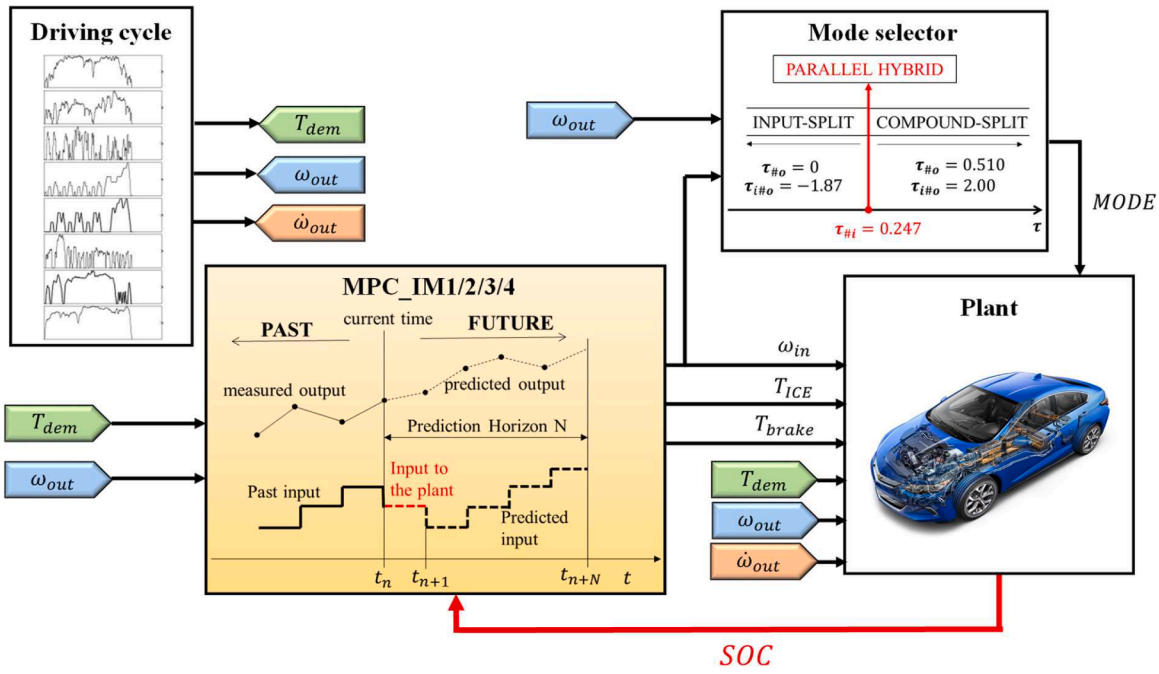


**Fig. 10.** Simulink backward-facing model for MPC EMS with integrated mode shift.

## 5. MPC problem formulation

MPC-based EMS allows solving multi-input multi-output nonlinear problems with equality and/or inequality constraints. The formulation of the MPC optimal control problem requires the following state-space representation of the controlled system, with state vector $\boldsymbol{x}(t)$, output vector $\boldsymbol{y}(t)$, and control vector $\boldsymbol{u}(t)$, for given external inputs $\boldsymbol{w}(t)$:

$$\begin{cases} \dot{\boldsymbol{x}}(t) = f(\boldsymbol{x}, \boldsymbol{u}, \boldsymbol{w}) y(t) = g(\boldsymbol{x}, \boldsymbol{u}, \boldsymbol{w}) \end{cases} \tag{25}$$

When applied to power-split HEVs to solve the EMS problem, the formulation based on the powertrain model of Section 2.1 involves the following vectors if the inertial load of the actuators is neglected:

$$\begin{cases} x(t) = \{SOC\} \\ u(t) = \{\omega_{in}, T_{ICE}, T_{brake}\} \\ y(t) = \{\dot{m}_{fuel}, SOC\} w(t) = \{\omega_{out}, T_{dem}\} \end{cases} \tag{26}$$

Thus, the nonlinear state-space equation is Eq. (16).

The goal of the MPC strategy is to establish the optimal control variables to minimise a cost function over a prediction horizon (PH). The cost function is defined as the sum of a first term penalising the ICE fuel rate, and a second term penalising the deviation of the battery SOC from a reference value:

$$J(\boldsymbol{x}, \boldsymbol{u}, \boldsymbol{w}, t) = \int_{t_o}^{t_0+PH} \left( q_1 \cdot \left| \dot{m}_{fuel} \right|^2 + q_2 \cdot \left| SOC - SOC_{ref} \right|^2 \right) dt \tag{27}$$

where $q_1$ and $q_2$ are the weights of the fuel rate and battery SOC deviation. The control variables optimisation must comply with the soft and hard constraints of the system, related to the battery SOC and power, and actuators speed and torque. Moreover, the mechanical braking torque, $T_{brake}$, must be positive to meet the adopted sign convention:

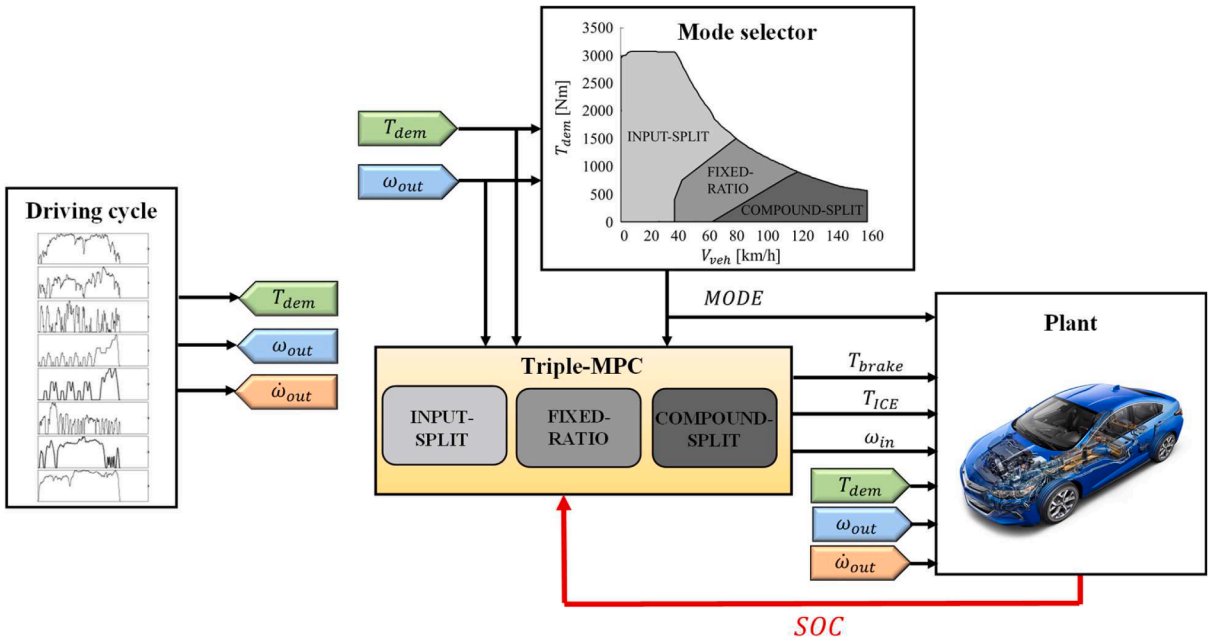


**Fig. 11.** Simulink backward-facing model for MPC EMS with pre-defined map for mode shift.

$$\begin{cases} SOC^{min} \leq SOC(t) \leq SOC^{max} \ (soft) \\ P_{batt}^{min} \leq P_{batt}(t) \leq P_{batt}^{max} \\ \omega_k^{min} \leq \omega_k(t) \leq \omega_k^{max} \\ T_k^{min} \leq T_k(t) \leq T_k^{max} \\ T_{brake} \geq 0 \end{cases} \tag{28}$$

with $k = ICE, MGA, MGB$. A soft constraint is considered on the battery SOC to ensure a deviation of around ±1 % from the 16 % reference value. When the optimal sequence of control inputs over the prediction horizon is obtained, the control variables assessed for the first time step are applied to the plant; then, the prediction horizon is moved one step forward and the optimisation is repeated for the next time step.

The MPC optimal control problem was set by implementing the equations of Sections 2 and 3 that were modified according to Table 7 in the Automatic Control and Dynamic Optimization toolkit (ACADO). ACADO is an open-source framework to solve optimal control problems using a solver based on sequential quadratic programming, combining gradient-based algorithms and quadratic programming to iteratively solve the optimal control problem also in real time [57]. The multiple-shooting discretisation and the Gauss-Newton Hessian approximation were set in the ACADO programming. Then, from the C++ code developed in the ACADO toolkit for MATLAB, an S-function is exported and embedded into the backward-facing Simulink framework in Fig. 10.

Embedding in the MPC internal model the universal formulation of Section 2.1 and the continuous switching formulation of Section 3.1 results in the following novelties: (1) a single controller is sufficient to deal with the EMS of any multimode power-spit powertrain, and (2) the possibility of performing a mode switch is integrated within the MPC framework, thus, there is no need of predefining the operating mode as input of the controller. The vehicle speed and demanded torque derived from the driving cycle are provided to the MPC block as external inputs to the controller. The MPC algorithm optimises the control variables, which include also the ICE speed, by initially supposing their first-attempt values and then changing them to pursue the minimisation of the cost function. For a given vehicle speed, the ICE speed affects the overall speed ratio, which determines the selected mode Section 3.1). Thus, a first-attempt mode is implicitly supposed in the optimisation through the first-attempt ICE speed, but then the considered mode varies if a different engine speed is considered by the optimisation algorithm, thanks to the continuous switching formulation of Eqs. (18) and ((19). Similarly, the optimal ICE speed returned by the MPC block determines the optimal transmission ratio and, thus, the selection of the optimal mode according to the strategy in Fig. 3. Therefore, the active mode is the result of the MPC optimisation. The optimal ICE

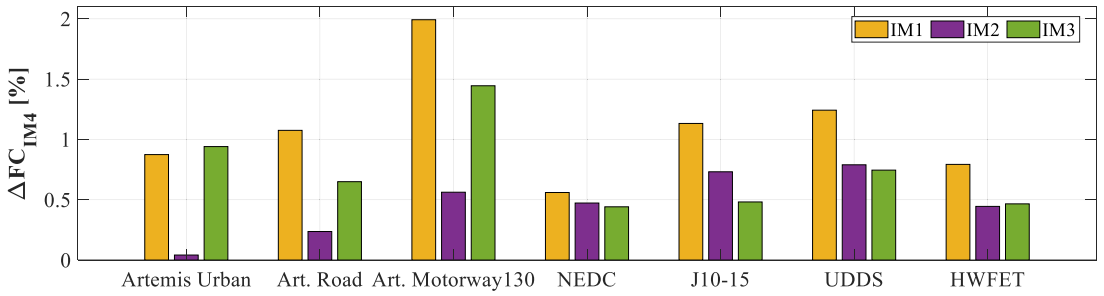


**Fig. 12.** Total fuel consumption: comparison of the simpler internal models versus IM4.

operations, PSU mode, and eventual friction braking torque are used as input data to the plant. The resulting battery SOC is provided in feedback to the MPC.

A benchmark MPC controller is introduced to test the performance of the novel internal model with integrated mode shift modelled by switch functions. The benchmarking MPC framework, shown in Fig. 11 and referred to as Triple-MPC, relies on the typical approach adopted in the literature based on multiple MPC controllers, one for each mode. Each controller is involved according to the current mode, which is selected on the basis of the demanded torque and vehicle speed by a mode selection map obtained from earlier offline analysis. In this case, the map provided by General Motors in [53] for the Chevrolet Volt operation is considered. Now the mode is a discrete external input to the MPC formulation, and not an optimised output. The internal model used for the IS and CS modes is formulated according to the same parametric approach of Section 2.1, by keeping constant values of the functional parameters in Table 3. The FR internal model is modified according to Eq. (17); thus, the ICE speed is proportional to the vehicle speed instead of a control variable.

A typical MPC internal model based on the Willis formula and PG free body diagram would not have allowed an integrated continuous formulation of the mode switch. On the contrary, the universal parametric model offers the opportunity to integrate the mode switch in the MPC optimal control problem or use a different optimisation strategy for mode selection.

## 6. Results and discussion

The MPC framework of Fig. 10 was implemented in Simulink to compare the performance of the four internal models with different complexity (Table 7) for the driving cycles of Table 6. A sampling time of 1 s and a prediction horizon of 10 s were used for the MPC controller. A brute-force optimisation was carried out to fit the cost function weights; the best performance was achieved when the minimisation of the fuel consumption was prioritised over the battery SOC variation through a weight one order of magnitude larger. A preview function was implemented to provide the MPC controller with future information on demanded torque and vehicle speed derived from the driving cycle.

To consider the different battery SOC at the end of the driving cycle, a fuel compensation term, $m_{fuel}^{comp}$, is added to the actual fuel consumption of the petrol engine, $m_{fuel}$ [58]. The total equivalent consumption $m_{fuel}^{eq}$ expressed in grams is:

$$m_{fuel}^{eq} = m_{fuel} + m_{fuel}^{comp} = m_{fuel} - \frac{\left(SOC_{end} - SOC_{ref}\right) Q_{batt} V_{OC} \overline{BSFC}}{1000} \tag{29}$$

where $m_{fuel}$ is the fuel consumption of the internal combustion engine in grams, $SOC_{end}$ is the final battery SOC ranging from 0 to 1, $SOC_{ref}$ is the reference SOC equal to 0.16, $\overline{BSFC}$ is the average brake specific fuel consumption of the engine expressed in g/kWh and equal to:

$$\overline{BSFC} = \frac{1}{\overline{\eta}_{ICE} H_{LHV}} \tag{30}$$

where $\overline{\eta}_{ICE}$ is the engine average efficiency over the driving cycle and $H_{LHV} = 0.01193$ kWh/g is the petrol lower heating value. The fuel consumption can be expressed in litres per 100 km as follows:

$$FC = \frac{m_{fuel}^{eq}}{d \rho_{fuel}} * 100 \tag{31}$$

where $d$ is the total distance covered by the driving cycle in km (Table 6) and $\rho_{fuel} = 743$ g/l is the petrol density.

The comparison between the four internal models of Table 7 is performed by considering the percentage variation from the most accurate internal models, i.e., IM4:

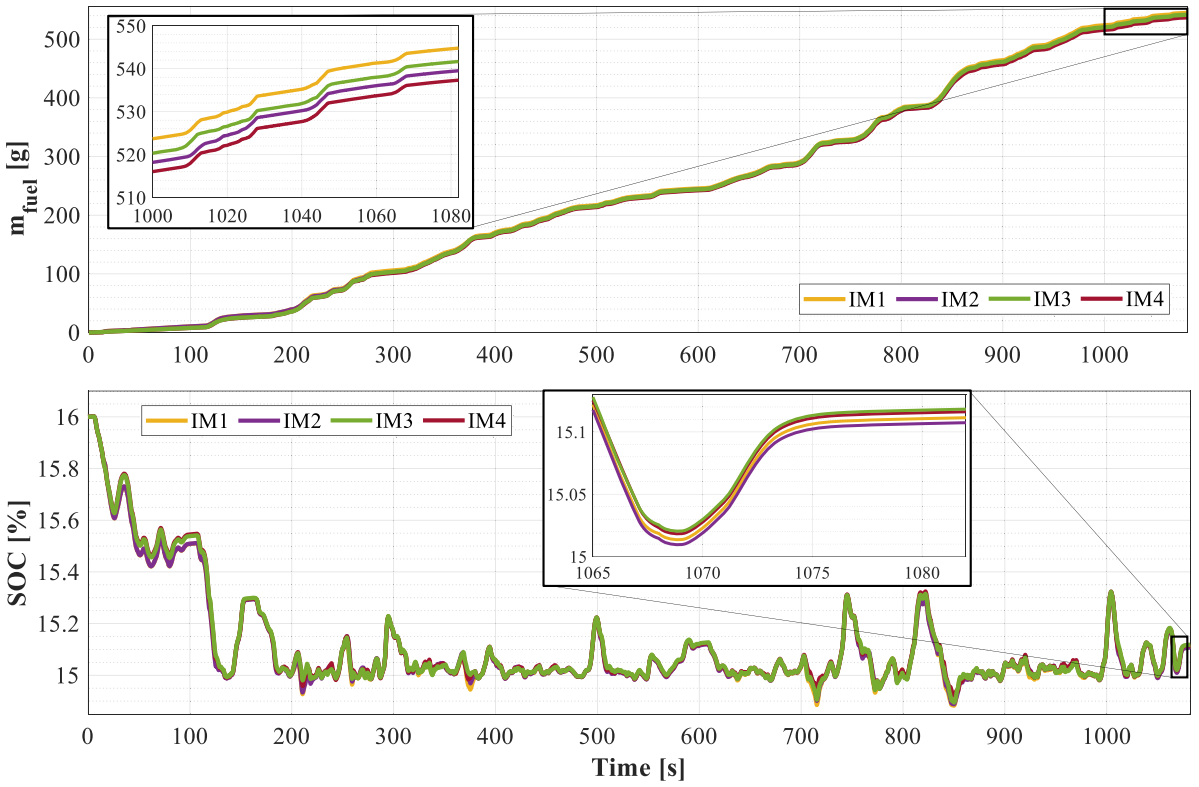


**Fig. 13.** ICE fuel consumption and battery SOC trends for each internal model in the Artemis Road cycle.

$$\Delta FC_{IM4,IM_j} = \frac{FC_{IM_j} - FC_{IM4}}{FC_{IM4}} \cdot 100 \tag{32}$$

with $j = 1, 2, 3$.

The results in Fig. 12 prove that the most accurate internal model IM4 always overperforms the other ones, since the percentage variation of Eq. (32) is positive in all the simulated driving cycles. Similarly, the simplest internal model IM1, which neglects the PSU meshing losses and considers a constant value for the MGs efficiency, leads to the highest fuel consumption, up to 2 % more than IM4 in the Artemis Motorway130 cycle. The Artemis Urban is an exception, since IM3 has the worst performance.

The performance assessment of the internal models IM2 and IM3 is less intuitive. IM2 results in the lowest variation from IM4 in the Artemis and HWFET cycles, while IM3 is the second-best internal model after IM4 in the NEDC, J10–15, and UDDS cycles. It should be noted that IM3 differ from IM4 for MGs efficiency, considered constant in IM3; on the other hand, IM2 differ from IM4 for PSU meshing losses, neglected in IM2. Therefore, the higher the difference between IM4 and IM3, the more the MGs efficiency affects the MPC performance; on the contrary, the higher the difference between IM4 and IM2, the more the PSU meshing losses affect the MPC performance. Hence, the EMS outcomes are more affected by the MGs efficiency in the Artemis and HWFET cycles, while the PSU meshing losses are more impactful in the NEDC, J10–15, and UDDS cycles. Nonetheless, the comparison of IM4 and IM2 indicates that the influence of the sole PSU meshing losses is less than 1 %. This is due to the fact that the Voltec II is a well-designed PSU, because the PGs synchronism is included within their actual working range [56]. Thus, the meshing losses are low for most operating conditions. Nevertheless, these results suggest that neglecting the PSU power losses during the design process outlined in Section 2.2 does not significantly affect the MPC-based EMS performance; hence, in the first instance, the meshing power losses can be neglected during the identification of the optimal functional parameters. As a result, any non-existing transmission can be modelled by only functional parameters without the need to define the constructive layout first. Then, after selecting the optimal functional parameters, the arrangement of the PGs can be defined through the design chart, so that they operate synchronously within the desired range to pursue low meshing losses. However, including PSU meshing losses in the MPC internal model for the EMS implementation is advisable to enhance fuel saving.

The above considerations might seem to contradict the results of the preliminary open-loop comparison (Fig. 8), where the impact of the PSU meshing losses is significantly higher. Nonetheless, the consideration of the different principles underpinning the MPC strategy and the ICE rule-based strategy is essential for a fair comparison between the MPC and the open-loop framework. Indeed, although the rule-based strategy attempts to limit the SOC variation, no constraints are imposed on it, thus exceeding the desired $\pm 1$ % range (Fig. 9). Moreover, the ICE operation is not affected by the internal model complexity in the open-loop framework. On the

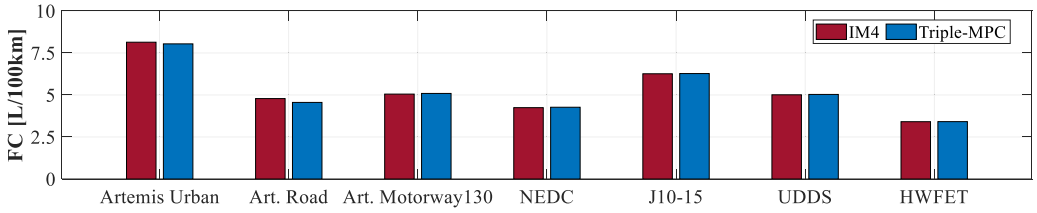


**Fig. 14.** IM4 with integrated mode switch versus Triple-MPC with offline mode optimisation strategy: fuel consumption comparison.

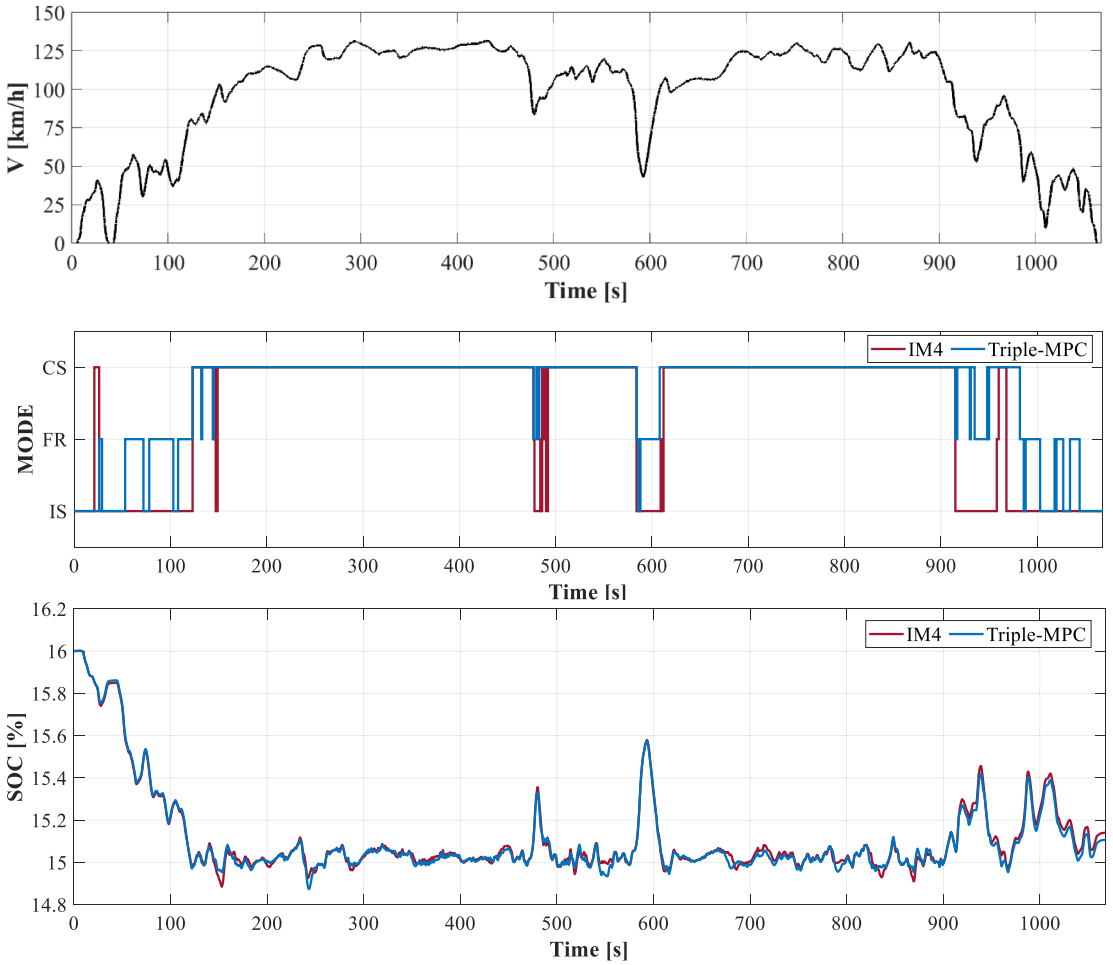


**Fig. 15.** IM4 with integrated mode switch versus Triple-MPC with offline mode optimisation strategy in the Artemis Motorway130 cycle: speed profile, mode, and battery SOC.

contrary, the MPC strategy instantaneously selects the best ICE operation to meet the constraint on the battery SOC, resulting into a total equivalent consumption affected by both fuel consumption and final SOC (Eq. (29)).

The actual ICE fuel consumption and final battery SOC are analysed to evaluate the impact of MGs efficiency and PSU meshing losses on the total equivalent consumption. The only Artemis Road results are reported in Fig. 13 for brevity. The graph shows that the engine fuel consumption is lower for IM4 and IM2, i.e., the internal models which include the polynomial MGs efficiency; on the contrary, the final battery SOC is higher if the PSU meshing losses are included in the IMs, i.e., in IM4 and IM3. The same trends for the ICE fuel consumption are detected for all the driving cycles except for Artemis Urban, where IM2 results in the lowest consumption, followed by IM4, IM1 and IM3. Regarding the battery SOC, the highest final value is always reached for IM4 or IM3, while IM2 and IM1 perform worse, according to the prediction of the open-loop analysis, whereby the PSU losses affect the battery SOC more than the MGs efficiency. Even a small difference in battery SOC affects the fuel compensation term in Eq. (29) because of the high energy storable in the battery and the low ICE efficiency. These results reveal the synergetic effect of including both polynomial MGs efficiency and PSU

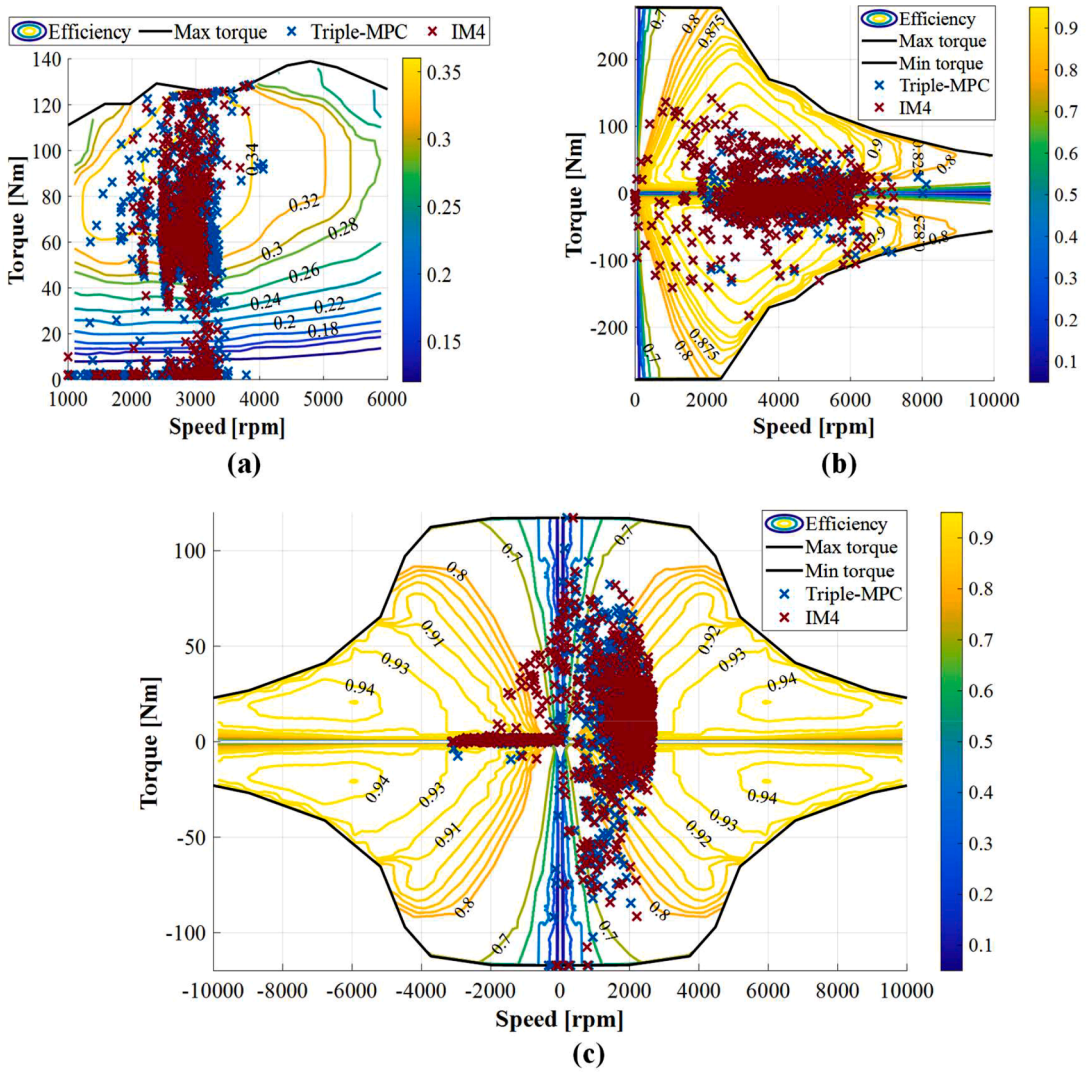


**Fig. 16.** IM4 with integrated mode switch versus Triple-MPC with offline mode optimisation strategy in the Artemis Motorway130 cycle: **(a)** ICE operations; **(b)** MGB operations; **(c)** MGA operations.

meshing losses in the MPC internal model, which leads to the IM4 best performance in terms of both fuel consumption reduction and final battery SOC increase.

Lastly, the Triple-MPC framework of Fig. 11 was implemented to compare the performance of the integrated mode switch against the mode selection strategy based on offline optimisation. Fig. 14 shows the difference in fuel consumption per 100 km of the internal model IM4 and the Triple-MPC framework. The integrated mode switch of IM4 fails to achieve the best powertrain operations in two driving cycles, i.e., the Artemis Urban and Road. Instead, it performs slightly better than the offline mode optimisation in the remaining five cycles. Therefore, the performance of the two controllers is comparable. On the one hand, this implies that adopting the novel formulation for online EMS of power-split HEVs may be worthy only if the switch functions of Eqs. (18) and (19) do not excessively increase the computational effort. Thus, further investigation of real-time capability is necessary, but it goes beyond the scope of this work. On the other hand, the lack of the need for offline optimisation would significantly reduce the computational time necessary to compare several viable solutions, making the integrated mode switch strongly preferable in the design stage.

To complete the comparison between IM4 and the Triple-MPC, the speed profile, the selected mode, and the battery SOC in the Artemis Motorway130 are shown in Fig. 15. IM4 and Triple-MPC differ in selecting the fixed-ratio mode for low-medium speed at the beginning and end of the driving cycle, resulting in slightly different usage of the battery power. Minor differences have been detected also in the operating points of the ICE and MGs, as shown in Fig. 16. In particular, the more frequent selection of the input-split mode performed by the controller IM4 when the vehicle speed is steeply variable (see Fig. 15), results in a higher variation of the MGB speed (see Fig. 16(b)), since it is kinematically coupled to the wheels in the input-split mode.

## 7. Conclusions

A universal parametric approach was rearranged and adopted as the internal model for an MPC-based energy management strategy for multimode power-split hybrid electric powertrains. The mathematical treatment relies on a unique formulation that befits any power-split transmission, being ruled by functional parameters that assume different values according to the constructive arrangement. As a result, switch functions were introduced to propose a novel integration of the mode shift within the receding horizon framework, in contrast to the more common strategy based on offline mode optimisation.

Moreover, the parametric model allows a swift evaluation of the transmission meshing losses, which are usually challenging to include in an MPC internal model because of the case-specific formulations required to assess losses in planetary gearing. Given the potential influence that the accuracy of the MPC internal model may have on the EMS performance, a comparison of internal models with different complexity for power-split HEVs was proposed for the first time. The internal models to assess in the MPC framework were selected after a preliminary open-loop analysis. The simulations suggested that, besides the PSU meshing losses, the influence of electric machines efficiency was worthy of investigation, too, while the actuators inertial load is negligible. Thus, four internal models differing for null or variable PSU meshing losses and constant or polynomial-fitted MGs efficiency were compared for the charge-sustaining operation of the second generation of Chevrolet Volt. The results showed that the difference in fuel consumption between the simplest and the most complex internal model is 2 % at most. In particular, considering or neglecting PSU meshing losses affects battery exploitation more than MGs efficiency, which, instead, has a higher impact on the engine operation. Furthermore, the novel MPC formulation with the integrated mode switch was compared with a benchmark EMS relying on a predetermined mode shift map, resulting in comparable performance.

Given that the improvement in fuel saving is relatively minor for the increased complexity of internal models, further analysis on real-time performance would help to understand if the new MPC formulation with variable meshing losses, polynomial MGs efficiency maps and integrated mode switch is worthy of onboard implementation. Nonetheless, for the same reason, the results obtained in this work suggest that using a simplified internal model with ideal PSU and constant MGs efficiency does not involve a significant error in the estimation of overall fuel consumption. This may be useful during the design stage when the ultimate PSU constructive arrangement and the electric machines have not been selected yet.

The MPC formulation based on the parametric internal model presented in this paper paves the path for a novel design procedure for PS-CVTs. The strength of this approach is the possibility to simulate any existing and non-existing transmission, even multimode, by only varying the PSU main functional parameters and without requiring offline optimisation of the mode shift strategy. As a result, the proposed MPC framework could be integrated with an optimisation algorithm for PSU functional parameters that can be selected according to the best vehicle performance and fuel saving. Then, the electric unit sizing and PSU synthesis could be performed according to the best functional parameters so as to pursue actuators downsizing and PGs synchronism. Lastly, the most complex internal model could be used to select the best powertrain arrangement amongst different viable solutions. Thanks to the utmost generality of the described design approach, it can be adopted for any power-split powertrain, not only in the automotive field.

The deployment of the analysed MPC framework in the design stage is still under development and requires further research to optimise the search for the best functional parameters in multimode operations. Nonetheless, such an automated design approach would not be possible with a traditional PSU model relying on case-specific equations, because a variation of the internal model would be required for any change in the PSU.

## Declaration of Competing Interest

The authors declare that they have no known competing financial interests or personal relationships that could have appeared to influence the work reported in this paper.

## Data availability

Data will be made available on request.

## References

[1] C. Mi, M.A. Masrur, Hybrid Electric Vehicles: Principles and Applications with Practical Perspectives, 2nd ed., John Wiley & Sons Ltd., 2017. https://onlinelibrary.wiley.com/doi/book/10.1002/9781118970553.
[2] W. Zhuang, S. Li (Eben), X. Zhang, D. Kum, Z. Song, G. Yin, F. Ju, A survey of powertrain configuration studies on hybrid electric vehicles, Appl. Energy 262 (2020), 114553, https://doi.org/10.1016/j.apenergy.2020.114553.
[3] X. Zeng, J. Wang, Analysis and Design of the Power-Split Device for Hybrid Systems, Springer, Singapore, 2017, https://doi.org/10.1007/978-981-10-4272-0.
[4] B. Conlon, Comparative analysis of single and combined hybrid electrically variable transmission operating modes, SAE Tech. Pap. 114 (2005) 1265–1275, https://doi.org/10.4271/2005-01-1162.
[5] P. Mattsson, Continuously variable split-power transmissions with several modes, 1996.
[6] L. Wang, Y. Cui, F. Zhang, G. Li, Architectures of planetary hybrid powertrain system: review, classification and comparison, Energies 13 (2020), https://doi.org/10.3390/en13020329.
[7] W. Zhuang, X. Zhang, Y. Ding, L. Wang, X. Hu, Comparison of multi-mode hybrid powertrains with multiple planetary gears, Appl. Energy 178 (2016) 624–632, https://doi.org/10.1016/j.apenergy.2016.06.111.
[8] S. Onori, L. Serrao, G. Rizzoni, Hybrid Electric Vehicles Energy Management Strategies, Springer, London, 2016.

[9] M.F.M. Sabri, K.A. Danapalasingam, M.F. Rahmat, A review on hybrid electric vehicles architecture and energy management strategies, Renew. Sustain. Energy Rev. 53 (2016) 1433–1442, https://doi.org/10.1016/j.rser.2015.09.036.

[10] C.M. Martinez, X. Hu, D. Cao, E. Velenis, B. Gao, M. Wellers, Energy management in plug-in hybrid electric vehicles: recent progress and a connected vehicles perspective, IEEE Trans. Veh. Technol. 66 (2017) 4534–4549, https://doi.org/10.1109/TVT.2016.2582721.

[11] J.M. Maciejowski, Predictive Control: With Constraints, Prentice Hall, 2002.

[12] Y. Huang, H. Wang, A. Khajepour, H. He, J. Ji, Model predictive control power management strategies for HEVs: a review, J. Power Sources 341 (2017) 91–106, https://doi.org/10.1016/j.jpowsour.2016.11.106.

[13] X. Lü, S. Li, X.H. He, C. Xie, S. He, Y. Xu, J. Fang, M. Zhang, X. Yang, Hybrid electric vehicles: a review of energy management strategies based on model predictive control, J. Energy Storage 56 (2022), 106112, https://doi.org/10.1016/J.EST.2022.106112.

[14] U. Montanaro, S. Dixit, S. Fallah, M. Dianati, A. Stevens, D. Oxtoby, A. Mouzakitis, Towards connected autonomous driving: review of use-cases, Veh. Syst. Dyn. 57 (2019) 779–814, https://doi.org/10.1080/00423114.2018.1492142.

[15] J. Theunissen, A. Tota, P. Gruber, M. Dhaens, A. Sorniotti, Preview-based techniques for vehicle suspension control: a state-of-the-art review, Annu. Rev. Control 51 (2021) 206–235, https://doi.org/10.1016/J.ARCONTROL.2021.03.010.

[16] V. Vidal, P. Stano, G. Tavolo, M. Dhaens, D. Tavernini, P. Gruber, A. Sorniotti, On pre-emptive in-wheel motor control for reducing the longitudinal acceleration oscillations caused by road irregularities, IEEE Trans. Veh. Technol. 71 (2022) 9322–9337, https://doi.org/10.1109/TVT.2022.3172172.

[17] A. Scamarcio, C. Caponio, M. Mihalkov, P. Georgiev, J. Ahmadi, K.M. So, D. Tavernini, A. Sorniotti, Predictive anti-jerk and traction control for V2X connected electric vehicles with central motor and open differential, IEEE Trans. Veh. Technol. (2022), https://doi.org/10.1109/TVT.2022.3143497.

[18] W. Golebiewski, K. Prajwowski, K. Danilecki, M. Lisowski, K.F. Abramek, Reducing the fuel consumption of an hybrid electric vehicle with the use of model predictive control - case study, IEEE Trans. Veh. Technol. (2023), https://doi.org/10.1109/TVT.2023.3266829.

[19] C. Sun, S.J. Moura, X. Hu, J.K. Hedrick, F. Sun, Dynamic traffic feedback data enabled energy management in plug-in hybrid electric vehicles, IEEE Trans. Control Syst. Technol. 23 (2015) 1075–1086, https://doi.org/10.1109/TCST.2014.2361294.

[20] C. Sun, X. Hu, S.J. Moura, F. Sun, Velocity predictors for predictive energy management in hybrid electric vehicles, IEEE Trans. Control Syst. Technol. 23 (2015) 1197–1204, https://doi.org/10.1109/TCST.2014.2359176.

[21] D. Yang, T. Liu, D. Song, X. Zhang, X. Zeng, A real time multi-objective optimization Guided-MPC strategy for power-split hybrid electric bus based on velocity prediction, Energy 276 (2023), https://doi.org/10.1016/J.ENERGY.2023.127583.

[22] X. Yang, C. Jiang, M. Zhou, H. Hu, Bi-level energy management strategy for power-split plug-in hybrid electric vehicles: a reinforcement learning approach for prediction and control, Front. Energy Res. 11 (2023) 183, https://doi.org/10.3389/FENRG.2023.1153390/BIBTEX.

[23] N. Yang, S. Ruan, L. Han, H. Liu, L. Guo, C. Xiang, Reinforcement learning-based real-time intelligent energy management for hybrid electric vehicles in a model predictive control framework, Energy 270 (2023), 126971, https://doi.org/10.1016/J.ENERGY.2023.126971.

[24] C. Le Xiang, F. Ding, W. Da Wang, W. He, Y.L. Qi, MPC-based energy management with adaptive Markov-chain prediction for a dual-mode hybrid electric vehicle, Sci. China Technol. Sci. 60 (2017) 737–748, https://doi.org/10.1007/s11431-016-0640-2.

[25] C. Xiang, F. Ding, W. Wang, W. He, Energy management of a dual-mode power-split hybrid electric vehicle based on velocity prediction and nonlinear model predictive control, Appl. Energy 189 (2017) 640–653, https://doi.org/10.1016/j.apenergy.2016.12.056.

[26] J. Guo, H. He, C. Sun, ARIMA-based road gradient and vehicle velocity prediction for hybrid electric vehicle energy management, IEEE Trans. Veh. Technol. 68 (2019) 5309–5320, https://doi.org/10.1109/TVT.2019.2912893.

[27] J. Oncken, B. Chen, Real-time model predictive powertrain control for a connected plug-in hybrid electric vehicle, IEEE Trans. Veh. Technol. 69 (2020) 8420–8432, https://doi.org/10.1109/TVT.2020.3000471.

[28] Z. Chen, H. Hu, Y. Wu, Y. Zhang, G. Li, Y. Liu, Stochastic model predictive control for energy management of power-split plug-in hybrid electric vehicles based on reinforcement learning, Energy 211 (2020), https://doi.org/10.1016/j.energy.2020.118931.

[29] B. Zhang, J. Zhang, F. Xu, T. Shen, Optimal control of power-split hybrid electric powertrains with minimization of energy consumption, Appl. Energy 266 (2020), 114873, https://doi.org/10.1016/J.APENERGY.2020.114873.

[30] J. Oncken, K. Sachdeva, H. Wang, B. Chen, Integrated predictive powertrain control for a multimode plug-in hybrid electric vehicle, IEEE/ASME Trans. Mechatron. 26 (2021) 1248–1259, https://doi.org/10.1109/TMECH.2021.3061287.

[31] W. Wang, X. Guo, C. Yang, Y. Zhang, Y. Zhao, D. Huang, C. Xiang, A multi-objective optimization energy management strategy for power split HEV based on velocity prediction, Energy 238 (2022), 121714, https://doi.org/10.1016/J.ENERGY.2021.121714.

[32] J. Zhang, T. Shen, Real-time fuel economy optimization with nonlinear MPC for PHEVs, IEEE Trans. Control Syst. Technol. 24 (2016) 2167–2175, https://doi.org/10.1109/TCST.2016.2517130.

[33] K. Yu, H. Yang, X. Tan, T. Kawabe, Y. Guo, Q. Liang, Z. Fu, Z. Zheng, Model predictive control for hybrid electric vehicle platooning using slope information, IEEE Trans. Intell. Transp. Syst. 17 (2016) 1894–1909, https://doi.org/10.1109/TITS.2015.2513766.

[34] W. Wang, C. Xiang, H. Liu, S. Jia, A model-predictive-control-based power management strategy for a power-split electromechanical transmission, Proc. Inst. Mech. Eng. Part D J. Automob. Eng. 230 (2016) 1987–2001, https://doi.org/10.1177/0954407016630911.

[35] X. Li, L. Han, H. Liu, W. Wang, C. Xiang, Real-time optimal energy management strategy for a dual-mode power-split hybrid electric vehicle based on an explicit model predictive control algorithm, Energy 172 (2019) 1161–1178, https://doi.org/10.1016/j.energy.2019.01.052.

[36] H. Wang, J. Oncken, B. Chen, Receding horizon control for mode selection and powertrain control of a multi-mode hybrid electric vehicle, in: Proceedings of the IEEE Conference on Vehicular Technology, 2019, https://doi.org/10.1109/VTCFALL.2019.8891382.

[37] R. Yang, X. Yang, W. Huang, S. Zhang, Energy management of the power-split hybrid electric city bus based on the stochastic model predictive control, IEEE Access 9 (2021) 2055–2071, https://doi.org/10.1109/ACCESS.2020.3047113.

[38] Z. Chen, H. Gu, S. Shen, J. Shen, Energy management strategy for power-split plug-in hybrid electric vehicle based on MPC and double Q-learning, Energy 245 (2022), 123182, https://doi.org/10.1016/J.ENERGY.2022.123182.

[39] F. Ju, N. Murgovski, W. Zhuang, X. Hu, Z. Song, L. Wang, Predictive energy management with engine switching control for hybrid electric vehicle via ADMM, Energy 263 (2023), 125971, https://doi.org/10.1016/J.ENERGY.2022.125971.

[40] A. Kahraman, D.R. Hilty, A. Singh, An experimental investigation of spin power losses of a planetary gear set, Mech. Mach. Theory 86 (2015) 48–61, https://doi.org/10.1016/j.mechmachtheory.2014.12.003.

[41] D.C. Talbot, A. Kahraman, A. Singh, An experimental investigation of the efficiency of planetary gear sets, J. Mech. Des. 134 (2012), https://doi.org/10.1115/1.4005599.

[42] C. Nutakor, A. Kłodowski, J. Sopanen, A. Mikkola, J.I. Pedrero, Planetary gear sets power loss modeling: application to wind turbines, Tribol. Int. 105 (2017) 42–54, https://doi.org/10.1016/J.TRIBOINT.2016.09.029.

[43] J.M. del Castillo, The analytical expression of the efficiency of planetary gear trains, Mech. Mach. Theory 37 (2002) 197–214, https://doi.org/10.1016/S0094-114X(01)00077-5.

[44] M. Velardocchia, E. Bonisoli, E. Galvagno, A. Vigliani, A. Sorniotti, Efficiency of epicyclic gears in automated manual transmission systems, SAE Tech. Pap. 2007-Septe (2007). 10.4271/2007-24-0139.

[45] E.L. Esmail, E. Pennestrì, A.H. Juber, Power losses in two-degrees-of-freedom planetary gear trains: a critical analysis of Radzimovsky's formulas, Mech. Mach. Theory 128 (2018) 191–204, https://doi.org/10.1016/j.mechmachtheory.2018.05.015.

[46] F. Bottiglione, S. De Pinto, G. Mantriota, Infinitely variable transmissions in neutral gear: torque ratio and power re-circulation, Mech. Mach. Theory 74 (2014) 285–298, https://doi.org/10.1016/j.mechmachtheory.2013.12.017.

[47] A.K. Gupta, C.P. Ramanarayanan, Analysis of circulating power within hybrid electric vehicle transmissions, Mech. Mach. Theory 64 (2013) 131–143, https://doi.org/10.1016/j.mechmachtheory.2013.01.011.

[48] D. Rotella, M. Cammalleri, Power losses in power-split CVTs: a fast black-box approximate method, Mech. Mach. Theory 128 (2018) 528–543, https://doi.org/10.1016/j.mechmachtheory.2018.06.011.

[49] M. Cammalleri, D. Rotella, Functional design of power-split CVTs: an uncoupled hierarchical optimized model, Mech. Mach. Theory 116 (2017) 294–309, https://doi.org/10.1016/j.mechmachtheory.2017.06.003.
[50] M. Cammalleri, A. Castellano, Analysis of hybrid vehicle transmissions with any number of modes and planetary gearing : kinematics, power flows, mechanical power losses, Mech. Mach. Theory 162 (2021), 104350, https://doi.org/10.1016/j.mechmachtheory.2021.104350.
[51] A. Castellano, M. Cammalleri, Power losses minimization for optimal operating maps in power-split HEVs: a case study on the Chevrolet Volt, Appl. Sci. 11 (2021) 7779, https://doi.org/10.3390/app11177779.
[52] A. Castellano, D. Leone, M. Cammalleri, Design of a hybrid electric power-split transmission for braking energy recovery in a drilling rig, Designs 6 (2022) 74, https://doi.org/10.3390/designs6050074.
[53] B.M. Conlon, T. Blohm, M. Harpster, A. Holmes, M. Palardy, S. Tarnowsky, L. Zhou, The next generation “voltec” extended range EV propulsion system, SAE Int. J. Altern. Powertrains 4 (2015) 248–259, https://doi.org/10.4271/2015-01-1152.
[54] S. Jurkovic, K. Rahman, N. Patel, P. Savagian, Next generation voltec electric machines; design and optimization for performance and rare-earth mitigation, SAE Int. J. Altern. Powertrains. 4 (2015) 336–342, https://doi.org/10.4271/2015-01-1208.
[55] W. Zhuang, X. Zhang, D. Li, L. Wang, G. Yin, Mode shift map design and integrated energy management control of a multi-mode hybrid electric vehicle, Appl. Energy 204 (2017) 476–488, https://doi.org/10.1016/j.apenergy.2017.07.059.
[56] D. Rotella, M. Cammalleri, Direct analysis of power-split CVTs: a unified method, Mech. Mach. Theory 121 (2018) 116–127, https://doi.org/10.1016/j.mechmachtheory.2017.10.006.
[57] B. Houska, H.J. Ferreau, M. Diehl, ACADO toolkit–an open-source framework for automatic control and dynamic optimization, Optim. Control Appl. Methods 32 (2011) 298–312, https://doi.org/10.1002/OCA.939.
[58] Y. Liu, J. Li, M. Ye, D. Qin, Y. Zhang, Z. Lei, Optimal energy management strategy for a plug-in hybrid electric vehicle based on road grade information, Energies 10 (2017), https://doi.org/10.3390/en10040412.